ORIGINAL RESEARCH

A theoretical investigation of the structure of 2-nitropyridine-*N*-oxide and the dependency of the NO$_2$ torsional motion on the applied wavefunction and basis set

Marwan Dakkouri · Volker Typke

Abstract HF, B3LYP, and MP2 wave functions in combination with Pople 6-31, 6-311 augmented with polarization functions on all atoms and Dunning double- and triple-zeta basis sets have been employed to investigate the structures and torsional potential function of the nitro group in 2-nitropyridine-*N*-oxide (2-NPO) and a variety of its fluorinated derivatives. The augmentation of the basis sets with diffuse functions showed a marked effect on the profile and barriers of the NO$_2$ torsional potential. Depending on the applied model chemistry, the heterocyclic ring in some 2-NPOs has proved to be non-planar. The non-planarity of the ring was characterized by Cremer–Pople puckering amplitude Q. The disruption of the ring planarity in some NPOs was accounted for the distinctive reactivity and impact sensitivity of these heterocycles. Consistently, the NBO and the AIM analyses furnished clear evidence for the accentuated weakness of the C–NO$_2$ bond and provided evidence for the electronic interplay between the NO$_2$ group, the fluorine substituent and the heterocyclic ring. Deletion of all off-diagonal Fock-matrix elements (NOSTAR) to separate hyperconjugative stabilizing interactions from steric interactions was used. The effect of nitration and fluorination on the aromaticity of the studied 2-NPOs was investigated by using the NICS descriptors NICS(1) and NICS(1)$_{zz}$. These NICS indices have shown that the fluorination in *para* position to the nitro group exhibits the highest degree of aromaticity within the fluorinated 2-NPOs.

Introduction and motivation

Nitropyridine-*N*-oxide derivatives have received particular interest in chemistry and biotechnology due to their accentuated oxidizing properties, high polarity, and their versatility as simultaneous charge donors and acceptors. These properties have qualified these compounds to be widely used in various fields of applications, e.g., as organocatalysts for asymmetric allylation of aldehydes [1], as inhibitor of HIV-1 reverse transcriptase [2, 3], as anti-viral agent against various SARS coronavirus strains [4], as antiadhesive and quorum-sensing inhibitor, and as anti-fungal agent [5]. Recent studies have shown that pyridine-*N*-oxide derivatives are genotoxic. The genotoxicity of this class of compounds is a consequence of damaging to DNA by affecting enzymes involved in DNA replication and the subsequent possible cell mutation which may lead to cancer [6]. Due to the conjugation of the nitro group with the N-oxide functional fragment 2- and 4-nitropyridine-*N*-oxides have been known as versatile intermediates in organic synthesis [7–11].

The versatility of the N-oxide hetero arenes originates mainly from the capability of the electron-rich N-oxide

M. Dakkouri (✉)
Department of Electrochemistry, University of Ulm,
Ulm, Germany
e-mail: marwan.dakkouri@gmx.de

V. Typke
Communication and Information Center, University of Ulm,
Ulm, Germany
e-mail: volker.typke@uni-ulm.de

functional group to undergo different coordination interactions, i.e., hydrogen bonding, metal chelation and to act as bridging chromophores and π–π* push–pull molecular rectifiers.

Obviously, the substitution of pyridine-*N*-oxide with a strong electron withdrawing entity like the NO_2 functional group would lead to the alteration of the charge density distribution and the structural parameters within the heterocyclic system, and thus would widen the scope of its reactivity. The additional substitution of a ring hydrogen by a strong electronegative fluorine atom would certainly result in a sizable rearrangement of the electronic structure of the nitropyridine-*N*-oxide fragment. Depending on the relative positions of these electron withdrawing substituents to each other and to the N-oxide entity the impact of such kind of substitution on the reactivity of the entire molecule could be noticeable. Moreover, the insertion of the fluorine substituent to the nitropyridine-*N*-oxide leads to a marked distortion of the sterical arrangement of the nitro group and the ionicity of the N-oxide and N–O bonds of nitro group. Because of the proximity of these multifunctional substituents to each other and due to the electronic mediation of the aromatic system both, the deviation of the NO_2 and N-oxide groups from the co-planarity with the ring as well as the planarity of the heterocyclic ring itself are anticipated to be differently affected. The peculiar crowding of these particular substituents which are electronically coupled through the pyridine ring has qualified this class of multifunctional heteroarene compounds to become the focal point of interest for many researchers in different fields of applied sciences and technology. Nitro pyridine-*N*-oxides have been used in agriculture for plants growth rate regulation [12], in photonics like the design and development of new organic nonlinear optical (NLO) materials for frequency doubling by means of second-harmonic generation (SHG) [13–19].

Computational details

The wave functions HF, MP2, and B3LYP in combination with the 6-31, 6-311, and Dunning correlation consistent cc-pVDZ, cc-pVTZ basis sets with and without diffuse and polarization functions augmentation on all atoms have been used. All calculations were carried out by using the G09 [20] and MOLPRO [21] software.For the description of the ring-puckering motion in the six-membered rings we used the Cremer–Pople algorithm [22–25]:

$$z_j = (1/3)^{1/2} q_2 \cos(\varphi_2 + 2\pi(j-1)/3) \\ + (1/6)^{1/2} q_3 (-1)^{(j-1)} \quad (j = 1, \dots 6),$$

with the conditions: $\Sigma z_j = 0$ and $\Sigma z_j^2 = q_2^2 + q_3^2$, where z_j is the perpendicular displacement of the jth atom from the plane of the unpuckered "ring mean plane". q_2 and q_3 are the puckering amplitudes, and φ_2 is the phase angle of the pseudorotation. To more thoroughly understand the molecular interactions leading to the unique properties of this class of pyridine-*N*-oxide derivatives we decided to investigate the structure of these molecules as well as the intramolecular charge transfer between the N-oxy group, the nitro group, and the ring skeleton. The main objective of this work is, however, to explore the torsional motion of the NO_2 group and to shed light on the dependency of this potential function on the applied level of theory.

To explore more systematically the dependency of the degree of the alteration of the geometrical parameters on the spatial position of the nitro group relative to the N-oxy group, we studied the torsional motion of the NO_2 group in the 2-nitropyridine-*N*-oxide (2-NPO) by rotating it around the N_8–C_2 bond by ≥180°. Interesting variations of the structural parameters of the stable rotamers, which correspond to minima on the predicted potential energy hypersurface, were observed. To ensure that these rotamers represent real minima but not saddle points on the potential energy surface we carried out frequency calculations (here and for all molecules occurring in this work) and only rotamers with no imaginary frequencies were considered. These stable out-of-plane rotamers result from a competing electronic interplay between the repulsive N-oxy and NO_2 group interaction on one hand and the attractive N=O⋯H interaction on the other hand.

Results and discussion

Structure of 2-NPO

Our calculations have shown that surprisingly the insertion of the NO_2 group in the *ortho* position to the N-oxide fragment has no significant effect on the structural parameters of pyridine-oxide (PO). By applying the MP2/aug-cc-pVDZ chemistry, we found that the N-oxide bond in 2-NPO shortens only by 0.006 Å (Table 1) in comparison to PO (this work, supporting information Table S1) and the ring N–C_2, C_2–C_3, and C_3–C_4 bonds shorten only by 0.003, 0.003, and 0.004 Å, respectively (for atomic numbering see Fig. 1). The nitration of PO, however, exerts more distinct effect on the bonding angles. For instance the C_2–N_1–C_6 angle narrows by 1.7° and the N_1–C_2–C_3 angles widens by approximately 2.7° upon nitration of PO in *ortho* position. From Table 1 (in this table the Dunning's basis sets cc-pVDZ and cc-pVTZ are abbreviated as VDZ and

VTZ and as AVDZ and AVTZ after their augmentation with diffuse functions), it can be seen that the values obtained from the density functional wave function are generally smaller by 0.005–0.01 Å than those provided by the MP2 method except for two cases, i.e., C_2–N_8 and N_1–O_7, where the values are slightly larger. The variations of the bond angles as obtained from both methods are almost negligible. Only the N_1–C_2–N_8 bond angle widens by 3.3° when B3LYP/AVDZ is used. The application of the density functional method provides a second stable rotamer in addition to that one shown in Table 1 with a positive low frequency in which the O–N–O plane is perpendicular to the ring plane. However, the energy difference between the two rotamers of 0.02 kcal mol^{-1} is almost negligible which indicates that the appearance of a second rotamer most likely is an artifact generated by the density functional wave function and is due to the quite flat potential minimum as it will be shown later in this work. Strikingly, the MP2/AVDZ method suggests an eclipsed arrangement for the C_2–N_8 and N_1–O_7 bonds in contrast to all other levels of theory in Table 1 which provide a dihedral angle N_8–C_2–N_1–O_7 deviating from zero and the N_8–C_2 and N_1–O_7 bonds are no more co-planar. Maybe of interest to note that the total dipole moment of PO increases by about 3 Debye on nitration in *ortho* position (from 5.2 to 8.1 D for PO and 2-NPO, respectively) emphasizing the asymmetric distribution of charges within 2-NPO and its accentuated polarity.

From Table 1, it is evident that the augmentation of the cc-pVDZ basis set with diffuse functions leads to the alteration of some structural parameters. Particularly the N_1–O_7 bond length increases by 0.016 Å and the bonding angle N_1–C_2–N_8 decreases by 3.5° upon basis set augmentation (when MP2 is used). The bond lengths C_2–N_8 and N_8–O_9 change by approximately 0.015 Å and the bond angle N_1–C_2–N_8 narrows by 3.9° on augmentation of the cc-pVTZ basis set and using B3LYP method. The most noticeable alteration as a consequence of the addition

Table 1 Structural parameters of 2-nitropyridine-*N*-oxide (2-NPO) as obtained from MP2 and B3LYP wave functions in combination with cc-pVDZ (VDZ), aug-cc-pVDZ (AVDZ), cc-pVTZ (VTZ), and aug-cc-pVTZ (AVTZ) basis sets

	MP2/			B3LYP/			
	VDZ	AVDZ	VTZ	VDZ	AVDZ	VTZ	AVTZ
Bond lengths							
N_1–C_2	1.396	1.385	1.380	1.386	1.374	1.373	1.374
N_1–C_6	1.399	1.391	1.384	1.386	1.378	1.376	1.380
C_2–C_3	1.394	1.391	1.380	1.391	1.386	1.380	1.377
C_3–C_4	1.397	1.403	1.387	1.389	1.392	1.383	1.390
C_4–C_5	1.410	1.410	1.397	1.402	1.401	1.394	1.397
C_5–C_6	1.386	1.391	1.375	1.379	1.382	1.373	1.378
N_1–O_7	1.248	1.264	1.250	1.256	1.270	1.261	1.256
C_2–N_8	1.463	1.461	1.453	1.470	1.471	1.469	1.454
N_8–O_9	1.235	1.238	1.227	1.217	1.220	1.213	1.229
N_8–N_{10}	1.232	1.238	1.230	1.229	1.228	1.223	1.229
Bond angles							
C_6–N_1–C_2	115.7	116.7	116.0	116.4	117.0	116.6	116.5
O_7–N_1–C_2	123.4	121.2	122.8	123.6	122.3	122.8	122.4
N_1–C_2–C_3	123.1	123.9	123.4	122.5	123.1	122.9	123.9
N_1–C_2–N_8	117.1	113.6	116.1	118.6	116.9	117.6	113.6
C_2–N_8–O_9	117.3	116.5	116.9	118.4	117.5	117.7	116.5
C_2–N_8–O_{10}	115.8	116.5	116.2	115.4	116.0	115.8	116.5
O_9–N_8–O_{10}	126.8	127.1	126.8	126.1	126.4	126.4	126.6
Dihedral angles							
N_1–C_2–N_8–O_9	−45.0	−90.3	−55.8	−35.6	−58.1	−50.3	−90.3
N_1–C_2–N_8–O_{10}	137.5	90.2	126.4	147.2	124.8	132.8	90.2
N_8–C_2–N_1–O_7	4.3	0.0	4.9	−5.3	−4.8	5.8	4.9
Q[a]	0.018	0.00	0.017	0.018	0.018	0.020	0.019
μ (Debye)	8.1	8.1	7.7	5.9	6.7	6.4	6.6

[a] $Q = \mathrm{sqrt}(q_2{}^2 + q_3{}^2)$: q_2 and q_3 are puckering amplitudes of the pseudorotational subspace and of the inversional subspace, respectively [22, 23]

Fig. 1 Atomic numbering of pyridine-*N*-oxide, *ortho*-, *meta*-, *para*-nitropyridine-*N*-oxide

Pyridine-*N*-Oxide   2-Nitropyridine-*N*-Oxide   3-Nitropyridine-*N*-Oxide   4-Nitropyridine-*N*-Oxide
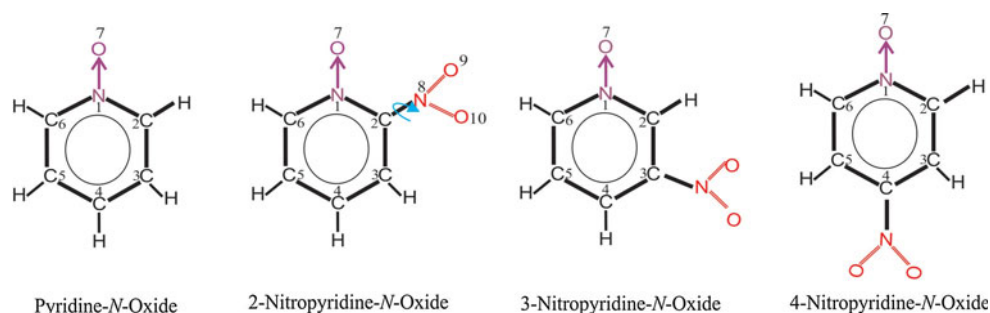
of diffuse functions is the change of the orientation of the NO_2 group from the *synclinal* (45°) to the *clinal* (90°) position and thus to a modification of the rotamer stability on the energy hypersurface.

To explore the impact of the direct adjacency of the nitro group and the N-oxide moiety and to gain more insight into the nature of the mutual interaction between these electron-rich groups, we found it of interest to compare some relevant structural parameters in 2-NPO with those in 3-NPO and 4-NPO where the nitro group is further apart from the N-oxide fragment (Fig. 1). The structural details of these nitropyridine-*N*-oxides along with the structural parameters of pentanitropyridine-*N*-oxide (PNPO) are listed in Table 2. The structure of PNPO was optimized to inspect the effect of crowding of the nitro groups on the structure and planarity of the heteroaromatic ring.

Inspection of Table 2 reveals that astonishingly the substitution of the nitro group in *ortho*, *meta*, or *para* position has no marked effect on the endocyclic bond lengths of the pyridine-*N*-oxide ring. However, the N-oxide bond length in all NPOs displayed in Table 2 (B3LYP/6-311++G(d,p)) shortens by 0.006–0.011 Å (and by 0.026 Å in PNPO) in comparison to pyridine-*N*-oxide (Table S1). At MP2/aug-cc-pVDZ level the N-oxide bond in 3-NPO shortens slightly, but the C-NO_2 bond elongates significantly by 0.021 Å in comparison to 2-NPO and 4-NPO (Table S3). Similar trend was also suggested by the B3LYP/aug-cc-pVDZ (Table S3) and by applying the same wave functions in combination with the 6-311++G(d,p) basis set (Table 2). This weakening of the C–NO_2 bond lends 3-NPO higher reactivity, and thus particular importance for technical and chemical applications. It is generally accepted that the C–NO_2 bond and its properties play a prominent role by the determination of the impact sensitivity of energetic materials [26–28]. As a result of the strong electron withdrawal ability of the NO_2 group, the angles including the anchor atoms widen substantially by approximately 3° and the C_2–N_1–C_6 angle increases by 2° in 2-NPO and remains unchanged in 3-NPO and 4-NPO in comparison to PO. Finally, as a consequence of the

proximity of the two electron-rich N-oxide and NO_2 groups in 2-NPO and the resulting electrostatic repulsive interaction between these groups the NO_2-plane adopt a perpendicular arrangement to the ring plane.

Recently, Li et al. [29] published a theoretical study of several polynitropyridines and pyridine-*N*-oxides. Among the structures which these authors have optimized by applying B3LYP/6-311++G(d,p) were 2-, 3-, and 4-nitropyridine-*N*-oxide. The endocyclic N_1–C_2, N_1–C_6, and the C–NO_2 bond lengths in these NPOs were found to be 1.374, 1.378, 1.472 Å in 2-NPO, 1.369, 1.377, 1.485 Å in 3-NPO, and 1.377, 1.377, 1.464 Å in 4-NPO, respectively (only these bond lengths were cited in this paper). A comparison of these values with those which have been produced by applying the MP2/6-311++G(d,p) method (Table 2) shows that the latter model chemistry predicts N_1–C_2, N_1–C_6 bond lengths which are longer by 0.010 and 0.012 Å in 2-NPO, 0.018, 0.015 Å in 3-NPO, and 0.011, 0.011 Å in 4-NPO. In contrast, the C–NO_2 bond length is shorter by 0.014, 0.007, and 0.002 Å in 2-NPO, 3-NPO, and 4-NPO, respectively. Similar result was obtained from the comparison of the computed structure of PNPO by applying B3LYP and MP2 wave functions in combination with the 6-311+G(d,p) basis set. As is evident from Table 2, the MP2/6-311+G(d,p) method provides a N_1–$C_{2(6)}$ bond length which is by 0.015 Å longer than that produced by the density functional method. However, the perturbation computational method suggests for the three C–NO_2 bond distances, $C_{2(3)(4)}$–NO_2 values which are by 0.022, 0.020, and 0.019 Å shorter than it was predicted by the B3LYP/6-311+G(d,p) levels. Interestingly, comparable behavior of the ring N–C and C–NO_2 bond lengths was obtained by applying the MP2 and B3LYP wave functions in combination with Dunning aug-cc-pVDZ basis set (Table S3). It is worth to point out that the crowding of the electron-rich substituents in PNPO leads to an apparent deviation of the ring skeleton from planarity, which is manifested in the puckering amplitude value of $Q = 0.028$ Å (Table 2) and the dihedral angle N_1–C_2–C_3–C_4 of 2.8°. Based on the above-demonstrated dependency of the C–NO_2 bond length on the employed level of theory, it is worth to indicate that using the

Table 2 Structural parameters of 2-nitropyridine-*N*-oxide (2-NPO), 3-nitropyridine-*N*-oxide (3-NPO), 4-nitropyridine-*N*-oxide (4-NPO), and penta-nitro-pyridine-*N*-oxide (PNPO), as obtained from MP2/6-311++G(d,p) and B3LYP/6-311++G(d,p)

	MP2/				B3LYP/			
	2-NPO	3-NPO	4-NPO	PNPO	2-NPO	3-NPO	4-NPO	PNPO
Bond lengths								
N_1–C_2	1.384	1.387	1.388	1.394	1.374	1.369	1.377	1.379
N_1–C_6	1.390	1.392	1.388	1.394	1.378	1.377	1.377	1.379
C_2–C_3	1.385	1.383	1.380	1.379	1.382	1.381	1.375	1.377
C_3–C_4	1.394	1.392	1.397	1.394	1.387	1.388	1.392	1.391
C_4–C_5	1.404	1.400	1.397	1.394	1.397	1.394	1.392	1.391
C_5–C_6	1.382	1.383	1.380	1.379	1.377	1.379	1.375	1.377
N_1–O_7	1.253	1.249	1.257	1.243	1.266	1.271	1.266	1.251
C_2–N_8	1.458			1.464	1.472			1.486
N_8–O_9	1.233			1.227	1.215			1.209
N_8–O_{10}	1.230			1.230	1.225			1.216
C_3–N_{11}		1.478		1.476		1.485		1.496
N_{11}–O_{12}		1.231		1.227		1.222		1.213
N_{11}–O_{13}		1.230		1.228		1.222		1.213
C_4–N_{14}			1.462	1.467			1.464	1.485
N_{14}–O_{15}			1.233	1.229			1.226	1.215
N_{14}–O_{16}			1.233	1.229			1.226	1.215
Bond angles								
C_2–N_1–C_6	116.0	118.1	118.2	115.3	116.7	118.6	118.9	116.6
C_2–N_1–O_7	122.4	120.8	120.9	122.3	122.6	120.7	120.5	121.7
N_1–C_2–C_3	123.7	119.7	121.7	122.9	123.2	119.9	121.3	122.4
C_2–C_3–C_4	119.5	123.6	119.2	120.8	119.6	122.8	119.2	120.4
C_3–C_4–C_5	117.7	115.5	120.0	117.4	117.9	116.3	119.9	117.8
C_4–C_5–C_6	121.1	121.7	119.2	120.8	120.7	120.9	119.2	120.4
C_5–C_6–N_1	121.9	121.3	121.7	122.9	121.9	121.6	121.3	122.4
N_1–C_2–N_8	115.3			114.3	117.1			114.2
C_2–N_8–O_9	116.4			115.7	117.6			115.9
O_9–N_8–O_{10}	126.7			128.6	126.4			128.7
C_2–C_3–N_{11}		117.0		118.3		117.6		118.5
C_3–N_{11}–O_{12}		117.3		115.5		117.5		115.5
O_{12}–N_{11}–O_{13}		125.9		128.3		125.4		128.4
C_3–C_4–N_{14}			120.0	121.3			120.0	121.1
C_4–N_{14}–O_{15}			117.3	116.0			117.5	116.0
O_{15}–N_{14}–O_{16}			125.3	127.9			125.0	127.9
Dihedral angles								
N_1–C_2–N_8–O_9	−118.4			69.1	54.9			72.0
N_1–C_2–N_8–O_{10}	63.3			−110.6	−128.2			−108.0
C_2–C_3–N_{11}–O_{12}		−21.3		−124.6		0.0		−124.6
C_2–C_3–N_{11}–O_{13}		158.8		55.0		180.0		54.4
C_3–C_4–N_{14}–O_{15}			−5.5	−131.8			0.0	−132.2
C_3–C_4–N_{14}–O_{16}			174.5	48.2			180.0	47.8
Q	0.017	0.006	0.000	0.021	0.020	0.000	0.000	0.028
μ (Debye)	8.2	5.1	0.6	0.4	6.9	4.4	1.2	0.2

Q puckering amplitude

computed lengthening of the C–NO$_2$ bond (and thus its weakening) is not primarily appropriate criterion for the determination of the impact sensitivity of energetic materials.

Chiang et al. [30] determined the structure of 4-NPO by means of the electron diffractions method. A comparison between the calculated structural parameters which we obtained from the MP2/aug-cc-pVDZ method with the experimentally determined values [30] reveals that the experimental values are quite unreasonable. So for instance, the electron diffraction study provided 1.281(22) and 1.469(66) Å for the N–O and C$_2$–N$_1$ bond distances, whereas our calculations predict 1.267 and 1.391 Å. Particularly striking is the C–NO$_2$ bond length of 1.628(13) Å versus our calculated value of 1.461 Å. All these evident discrepancies indicate that the experimental study of the structure of 4-NPO needs to be revisited. In the same electron diffraction investigation, the molecular structure of 4-chloropyridine-N-oxide (4-ClPO) was determined as well. The optimized structure 4-ClPO (MP2/aug-cc-pVDZ was used) revealed that reasonable agreement between the observed N-oxide bond length of 1.262(25) Å and the calculated value of 1.269 Å exists but a significant disagreement for all other structural parameters (differences of ±0.03 to ±0.05 Å for the bond lengths and up to 5° for the bond angles) is apparent which also necessitates the experimental reinvestigation of this molecule.

One of the peculiar features we obtained from this study is the non-planarity of the heteroaromatic ring upon nitration (and fluorination as it will be shown later in this work). Table 1 shows that the Cremer–Pople (CP) total puckering amplitude Q in all listed calculations varies between 0.017 and 0.020, except when Dunning's VDZ basis set augmented with diffuse functions is used the ring proves to be planar. Numerous papers have been published over the last four decades in which the reasons for the remarkable properties of nitropyridine-N-oxides and their derivatives have been investigated. Mainly intramolecular interactions of various kinds and charge redistribution as a result of substitution have been made accountable for their chemical reactivity, remarkable magnetic and optical properties, and versatile biological activity. However, to the best of our knowledge never before has the contribution of the non-planarity of these heteroaromatics been considered for the elucidation of these particular properties. We strongly believe that the enforced disruption of the planarity of these heterocyclic compounds and the resulting extra strain play a prominent role by the enhancement of the chemical and biological activity of this class of molecules, e.g., impact sensitivity for characterizing high energy density materials and genotoxicity.

The above-indicated disruption of the co-planarity between the NO$_2$ group and the ring as well as the

noticeable basis set dependency of the shape and multiplicity of the torsional potential of the nitro group have prompted us to successively substitute the ring hydrogen atoms by fluorine atoms to examine the influence of the incorporation of such strongly electronegative atom into the 2-NPO system on both, the structural parameters and the torsional motion of the nitro group. Such an effect is likely to anticipate since the charge shift towards the fluorine atom and its ability to hyperconjugate with the aromatic ring system by donating lone pair electrons into adjacent antibonding orbital (negative hyperconjugative interaction) and to exert exchange repulsive interaction (Pauli-repulsion) would contribute to pronounced charge density redistribution within the 2-NPO molecular system. In this context, we performed quantum chemical calculations at various level of model chemistry: 2-nitropyridine-X-Fluoro-N-oxide ($X = 3, 4, 5$, and 6) and 2-nitropyridine-3,4,5,6-tetrafluoro-N-oxide (2-NPO-F4).

Structures of 2-NPO-x-F

A comparison between the skeleton C–C and C–N bond distances in the 2-NPO (Table 1) and its fluorinated derivatives (Table 3, for atomic numbering see Fig. 2) shows that regardless the position and degree of fluorination these bond lengths remain almost unaffected. The consequences of the neighborhood of the fluorine atom to the N$_1$–O$_7$ bond in 2-NPO-6-F are: (i) shortening of the N$_1$–O$_7$ bond in comparison to the remaining fluoro derivatives, and (ii) narrowing of the C$_2$–N$_1$–C$_6$ bond angle (Table 3). Inspection of the NBO analysis results reveals that there is no direct electronic interaction between the fluorine atom and the adjacent oxygen atom. However, in the NBO space, the second-order perturbation energy for the $(n_\pi)_F \rightarrow \sigma^*_{(N_1-C_6)}$ charge delocalization is 12.1 kcal mol^{-1}. Therefore, the latter hyperconjugative interaction is the reason for the aforementioned alterations of the N$_1$–O$_7$ bond length and the C$_2$–N$_1$–C$_6$ bond angle. Further details of the NBO analysis will be discussed later in this work.

Remarkably, neither the successive monofluorination on all positions of the pyridine ring nor the tetrafluorination has a sizable effect on the bond lengths in comparison to the non-fluorinated 2-NPO. The largest variation of 0.009 Å is attributed to the C$_3$–C$_4$ bond length in 2-NPO-3-F and 2-NPO-4-F. On the other hand, while the C–F bond in 2-NPO-4-F and 2-NPO-5-F lengthens by 0.007 and 0.005 Å in comparison to 2-NPO-3-F, this bond shortens significantly by 0.019 Å in 2-NPO-6-F. Obviously, this latter bond contraction is due to hyperconjugative interactions with the neighboring N-oxide fragment. For the same reason while the expected shortening of the C–F bond is almost negligible upon the progressive fluorine substitution

Table 3 Structural parameters of the fluoro derivatives of 2-NPO: 2-NPO-X-Fluoro (X = 3, 4, 5, 6, and 3–4–5–6) as predicted by MP2/aug-cc-pVDZ

	2-NPO	2-NPO-3-F	2-NPO-4-F	2-NPO-5-F	2-NPO-6-F	2-NPO-F4
Bond lengths						
N_1–C_2	1.385	1.384	1.384	1.389	1.390	1.386
C_2–C_3	1.391	1.392	1.392	1.391	1.392	1.391
C_3–C_4	1.403	1.394	1.394	1.402	1.402	1.398
C_4–C_5	1.410	1.410	1.402	1.402	1.409	1.404
C_5–C_6	1.391	1.390	1.392	1.389	1.385	1.392
C_6–N_1	1.391	1.391	1.390	1.390	1.394	1.388
N_1–O_7	1.264	1.264	1.265	1.262	1.259	1.261
C_2–N_8	1.461	1.458	1.461	1.460	1.461	1.460
N_8–O_9	1.238	1.237	1.238	1.237	1.237	1.237
N_8–O_{10}	1.238	1.237	1.238	1.240	1.240	1.237
C_3–H(F)$_{11}$	1.090	1.351	1.092	1.092	1.092	1.342
C_4–H(F)$_{12}$	1.093	1.091	1.358	1.091	1.091	1.341
C_5–H(F)$_{13}$	1.093	1.092	1.092	1.356	1.092	1.340
C_6–H(F)$_{14}$	1.094	1.090	1.090	1.090	1.332	1.324
Bond angles						
C_6–N_1–C_2	116.7	117.1	116.7	116.8	115.0	116.3
O_7–N_1–C_2	121.2	120.6	121.2	122.0	123.1	122.0
N_1–C_2–C_3	123.9	122.3	124.2	123.3	124.1	123.2
N_1–C_2–N_8	113.6	115.1	113.7	115.3	114.2	114.6
C_2–C_3–C_4	119.1	121.3	117.4	120.2	119.3	120.1
C_3–C_4–C_5	117.8	116.2	120.4	116.0	118.2	117.5
C_4–C_5–C_6	121.2	121.9	119.5	123.3	119.8	120.8
C_5–C_6–N_1	121.4	121.2	121.8	120.3	123.6	122.2
F–C_3–C_2		117.4				119.3
F–C_3–C_4		121.2				120.6
F–C_4–C_3			119.8			121.6
F–C_4–C_5			119.8			120.9
F–C_5–C_4				119.6		120.3
F–C_5–C_6				117.1		119.0
F–C_6–N_1					113.6	115.7
F–C_6–C_5					122.7	122.1
C_2–N_8–O_9	116.5	116.3	116.4	116.8	116.6	116.1
C_2–N_8–O_{10}	116.5	116.3	116.4	116.3	116.4	116.1
O_9–N_8–O_{10}	127.1	127.5	127.3	126.9	127.0	127.8
Dihedral angles						
N_1–C_2–N_8–O_9	−90.3	−90.0	−90.1	−63.4	−66.9	−90.0
N_1–C_2–N_8–O_{10}	90.2	90.0	90.3	118.4	114.7	90.0
N_8–C_2–N_1–O_7	0.0	0.0	0.0	−3.5	−3.1	0.0
Q	0.00	0.00	0.00	0.015	0.012	0.0
μ (Debye)	8.1	8.0	6.5	6.3	8.2	4.8

Q puckering amplitude

in *meta* and *para* positions in 2-nitro-3,4,5,6-tetrafluoro-pyridine-*N*-oxide (2-NPO-F4) this shortening becomes notable (0.016 Å) for the C–F bond in *ortho* position. Such C–F bond shortening in 2-NPO-6-F and in 2-NPO-F4 is to

some extent surprising because the NBO analysis has predicted that the occupancy of the $\pi_{N_1-C_6}$ NBO remains almost constant in all monofluorinated 2-NPO, i.e., 1.722–1.728 electrons (in 2-NPO-F4 is 1.744 e$^-$). Similarly, the
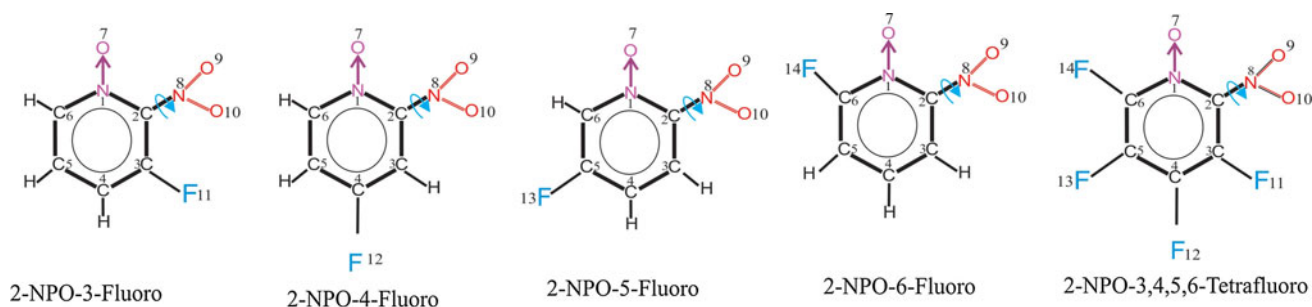
Fig. 2 Atomic numbering of mono- and tetra-fluorinated 2-nitropyridine-*N*-oxide

occupancy of the $\sigma_{N_1-C_{2,6}}$ NBOs varies only negligibly (1.979–1.983 e⁻). In this context, it is worth to indicate that the values of the exocyclic bond angles involving the fluorine substituent (Table 3) show that there is an attractive interaction between the fluorine atom and the nitro group in 3-NPO-3-F and rather more accentuated attractive interaction between the fluorine substituent and the N-oxide oxygen in 2-NPO-6-F and 2-NPO-F4. In these instances where the F⋯O distance is between 2.6 and 3.3 Å, it appears that the attractive fluorine–oxygen dispersion interaction is the predominant effect in comparison to the repulsive Pauli exchange interaction. This finding is in agreement with the very recently discussed importance of the dispersion energy by the stabilization of large molecules by means of intramolecular dispersion interaction between, e.g., functional groups [31]. Another intriguing feature is that the geometrical parameters of the nitro group in all fluorinated compounds which are shown in Table 3 are insensitive to the charge density variation of the heterocyclic ring as a consequence of the charge withdrawal by the fluorine atoms. The opening of the endocyclic angles involving the anchor atoms for the fluorine substitution can be explained by invoking the σ-electron withdrawing ability of the fluorine substituent.

In all fluorinated 2-NP-*N*-oxides in Table 3, the contribution of the σ-character to the natural atomic hybrid orbital of the carbon anchor atom on which fluorine is substituted amount only to 23–24 % indicating the loss of σ-electrons upon fluorination. In addition, as it will be shown later the second-order perturbation energy significantly favors the hyperconjugative bond–antibond interaction between the π_2 electron lone pair of the fluorine atom and the C_{anchor}–C antibond which contributes to the widening of these angles.

To investigate the effect of the electronegativity and the size of the halogen substituent on the geometrical parameters of the 2-nitro-*N*-oxide framework, the fluorine atom in 2-NPO-*x*-F series was substituted by a chlorine atom leading to the 2-NPO-*x*-chlorine homologues. Without

going into further details of the computational results, it is interesting to note that surprisingly except for few instances such a halogen substitution has generally a little effect on the bond lengths and bond angles of the 2-nitro-*N*-oxide moiety. Predominantly some bond distances and bond angles in 2-NPO-6-Cl and 2-NPO-Cl4 show some noticeable differences when compared to the fluorine counterparts. For instance by using the MP2/aug-cc-pVDZ method the N_1–C_6 and C_5–C_6 bond lengths in 2-NPO-6-Cl are by 0.008 and 0.011 Å longer than in 2-NPO-6-F. From the comparison of structural parameters of 2-NPO-Cl4 and 2-NPO-F4, it emerges that the N_1–C_6, C_3–C_4, C_4–C_5, and C_5–C_6 are by 0.016, 0.013, 0.012, and 0.013 Å, respectively, longer in the former than in the latter compound. It is also worth to note that the NO_2 plane in 2-NPO-6-Cl is perpendicular to the ring plane which is in contrast to the arrangement of the nitro group in the corresponding fluoro compound (Table 3). All these structural trends have also been reproduced by applying the B3LYP wave function and the Gaussian basis set 6-311++G(df,pd).

In a further attempt to separate the concerted effects of the fluorine and nitro group on the geometrical parameters of the pyridine-*N*-oxide skeleton and to learn more about the effective role of the nitro group by the charge redistribution within the ring skeleton we studied the structures of 2-fluoro-, 3-fluoro, 4-fluoro-, 3,4,5,6-tetrafluoro-, and penta-fluoro-pyridine-*N*-oxide. Table 4 summarizes the most important structural parameters of these fluorinated pyridine-*N*-oxides as suggested by the MP2/aug-cc-pVDZ calculations. From the comparison of Tables 3 and 4, it emerges that the absence of the nitro group has almost negligible effect on the ring bond distances. Conspicuously is that the N-oxide as well as the C–F bond lengths in all nitrated homologues are by 0.004 to 0.008 Å shorter than the corresponding bonds in the fluoro pyridine-*N*-oxide counterparts. In contrast to the bond lengths the endocyclic bond angles vary more significantly and non-uniform in both series. The largest variations show the angles N_1–C_2–C_3 and C_2–C_3–C_4. For instance, the N_1–C_2–C_3 angle in

2-NPO-3-F is by 2.5° larger and the C_2–C_3–C_4 angle is by 2.0° smaller than in 3-F-PO. Similarly, the former angle widens by 2.4° and the latter one narrows by 1.6° on moving from 2-NPO-6-F to 6-F-PO. Moreover, we note that the nitration of the fluoro-pyridine-N-oxides leads to the anticipated increase of the molecular dipole moment and the largest increase of 3.6 D occurs on going from 3-F-PO to 2-NPO-3-F.

Since the anticipated structural changes of the 2-NPO framework were not distinctively revealing for the

Table 4 Structural parameters of the fluoro derivatives of N-PO: x-F-PO (x = 2, 3, 4; 3,4,5,6-tetra- and 2,3,4,5,6-penta-) as predicted by MP2/aug-cc-pVDZ

	2-F-PO	3-F-PO	4-F-PO	Tetra-F-PO	Penta-F-PO
Bond lengths					
N_1–C_2	1.390	1.386	1.387	1.388	1.388
C_6–N_1	1.388	1.390	1.387	1.386	1.389
C_2–C_3	1.393	1.391	1.395	1.390	1.392
C_3–C_4	1.406	1.398	1.397	1.400	1.400
C_4–C_5	1.406	1.408	1.397	1.400	1.400
C_5–C_6	1.388	1.392	1.395	1.393	1.392
N_1–O_7	1.265	1.268	1.271	1.265	1.261
C_2–F_8	1.337				1.327
C_3–F_9		1.359		1.349	1.342
C_4–F_{10}			1.364	1.345	1.344
C_5–F_{11}				1.342	1.343
C_6–F_{12}				1.328	1.327
Bond angles					
C_6–N_1–C_2	116.7	118.7	118.4	117.6	116.5
O_7–N_1–C_2	122.0	120.5	120.8	121.8	121.8
N_1–C_2–C_3	121.7	119.8	121.6	120.9	122.6
C_2–C_3–C_4	120.9	123.3	119.2	121.9	120.3
C_3–C_4–C_5	117.7	115.6	120.1	116.9	117.8
C_4–C_5–C_6	119.6	121.7	119.2	120.6	120.4
F_8–C_2–C_3	122.3				122.0
F_8–C_2–N_1	114.4				115.5
F_9–C_3-C_2		116.0		118.8	119.1
F_9–C_3–C_4		119.8		119.3	120.6
F_{10}–C_4–C_3			120.0	122.0	121.2
F_{10}-C_4–C_5			120.0	121.0	121.1
F_{11}–C_5–C_4				120.4	120.5
F_{11}–C_5–C_6				119.0	119.1
F_{12}–C_6–C_5				121.7	122.0
F_{12}–C_6–N_1				116.2	115.4
μ (Debye)	6.2	4.4	3.4	2.8	3.3

electronic effects of clearly different kinds of substituents we decided to check whether the atomic and group charge distributions in the studied 2-NPOs provide more reliable supporting criteria for a better interpretation of these substituent/heteroaromatic interactions.

Regardless the controversy that has occasionally arisen about which is the best concept for describing the charge distribution between bonded atoms, we decided to use both the natural population analysis (NPA) [32] in the NBO space, and the Mulliken charge population analysis [33]. Nevertheless, for the following discussion, we will mainly focus on the natural charges despite the criticism that has been raised against the NPA method, e.g., assigning the electrons to lone pairs and core orbitals or to bonding and antibonding orbitals between atoms leads to an overestimation of atomic charges (and thus the bond polarity) and the molecular dipole moments [34–36]. However, based on our experience and the repeated comments that have been made by various authors, the Mulliken charge population has been known to be basis set dependent in contrast to natural charges and frequently underestimates the bond polarity [37, 38].

The calculated natural atomic charges and the Mulliken charges in pyridine-N-oxide and its nitrated and fluorinated derivatives as suggested by the B3LYP/aug-cc-pVDZ chemistry are shown in Tables 5 and 6 (for the computed natural and Mulliken atomic charges by applying different methods see Tables S5–S8). From Table 5, it is apparent that the insertion of the nitro group in *ortho* position to the N-oxide moiety results in a withdrawal of charges from the ring atoms and the N-oxide oxygen. The substitution of hydrogens in different positions of 2-NPO by a fluorine atom does not show a clear systematic variation of the charge distribution in this diversity of fluoro 2-NPO compounds. The reason for that could be the alteration of the charge distribution within the ring represents a compromise between two competing effects of substituents: the strong negative inductive and resonance effects of the nitro group (increased electron density in *meta* position) and the negative inductive and positive resonance effects of the fluorine atom (higher electron density in *ortho* and *para* positions). The largest loss of charges, however, shows the C_6 atom of +0.63 e[-] (+0.61 e[-] as produced by MP2/aug-cc-pVDZ, Table S5) in 2-NPO-6-F. Also in this compound, the charge of the N_1 atom of +0.007 e[-] (+0.03 e[-]) is close to neutrality and the N-oxide bond possesses a distinct polarity within this series of fluorinated 2-NPOs. As a result the N_1–O_7 and the C–F bonds of 1.259 and 1.332 Å (Table 3), respectively, are the shortest within the mono-fluorinated compounds. By applying the MP2/6-311++G(df,pd) computational method, these bond lengths are even shorter and amount to 1.246 and 1.307 Å.

Inspection of the charge population in 2-NPO-4-F reveals (Table 5) that the substitution of the fluorine atom

Table 5 Natural charges of pyridine-*N*-oxide (PO), 2-nitropyridine-*N*-oxide (2-NPO), 2-nitro-3-fluoropyridine-*N*-oxide (2-NPO-3-F), 2-nitro-4-fluoropyridine-*N*-oxide (2-NPO-4-F), 2-nitro-5-fluoropyridine-*N*-oxide (2-NPO-5-F), 2-nitro-6-fluoropyridine-*N*-oxide (2-NPO-6-F), and 2-nitro-3-4-5-6-tetrafluoropyridine-*N*-oxide (2-NPO-F4) as obtained from B3LYP/aug-cc-pVDZ

Atom	PO	2-NPO	2-NPO- 3-F	2-NPO-4-F	2-NPO-5-F	2-NPO-6-F	2-NPO-F4
N_1	0.049	0.053	0.058	0.035	0.069	0.007	0.011
C_2	−0.003	0.292	0.239	0.321	0.274	0.304	0.244
C_3	−0.241	−0.220	0.423	−0.291	−0.203	−0.239	0.366
C_4	−0.241	−0.229	−0.288	0.429	−0.291	−0.212	0.328
C_5	−0.241	−0.229	−0.223	−0.293	0.426	−0.293	0.315
C_6	−0.003	0.005	−0.005	0.023	−0.062	0.631	0.578
O_7	−0.542	−0.495	−0.499	−0.521	−0.469	−0.491	−0.486
N_8		0.487	0.495	0.491	0.483	0.488	0.493
O_9		−0.324	−0.326	−0.330	−0.322	−0.321	−0.315
O_{10}		−0.364	−0.326	−0.330	−0.374	−0.349	−0.315
H_8	0.246						
H_9	0.246						
H_{10}	0.239						
$F_{11}(H)$	0.246	0.267	−0.327	0.277	0.275	0.267	−0.308
$F_{12}(H)$	0.246	0.249	0.263	−0.338	0.264	0.252	−0.308
$F_{13}(H)$		0.253	0.257	0.268	−0.335	0.265	−0.307
$F_{14}(H)$		0.255	0.257	0.259	0.267	−0.309	−0.295

Table 6 Mulliken atomic charges of pyridine-*N*-oxide (PO), 2-nitropyridine-*N*-oxide (2-NPO), 2-nitro-3-fluoropyridine-*N*-oxide(2-NPO-3-F), 2-nitro-4-fluoropyridine-*N*-oxide (2-NPO-4-F), 2-nitro-5-fluoropyridine-*N*-oxide (2-NPO-5-F), 2-nitro-6-fluoropyridine-*N*-oxide (2-NPO-6-F), and 2-nitro-3-4-5-6-tetrafluoropyridine-*N*-oxide (2-NPO-F4) as obtained from B3LYP/aug-cc-pVDZ

Atom	PO	2-NPO	2-NPO-3-F	2-NPO-4-F	2-NPO-5-F	2-NPO-6-F	2-NPO-F4
N_1	0.294	0.313	0.224	0.244	0.292	0.231	0.170
C_2	0.455	0.055	0.224	−0.010	0.049	0.216	0.266
C_3	1.206	1.590	0.946	1.700	1.433	1.478	1.054
C_4	0.595	0.489	0.916	0.050	0.853	0.466	0.628
C_5	1.206	1.268	1.106	1.513	0.646	1.060	0.821
C_6	0.455	0.460	0.640	0.531	0.651	0.587	0.583
O_7	−0.836	−0.761	−0.766	−0.777	−0.733	−0.756	−0.740
N_8		0.542	0.491	0.525	0.574	0.526	0.504
O_9		−0.586	−0.588	−0.592	−0.587	−0.590	−0.579
O_{10}		−0.605	−0.588	−0.592	−0.621	−0.590	−0.579
H_8	−0.646						
H_9	−0.701						
H_{10}	−0.681						
$F_{11}(H)$	−0.701	−0.736	−0.573	−0.716	−0.738	−0.759	−0.575
$F_{12}(H)$	−0.646	−0.680	−0.672	−0.531	−0.667	−0.668	−0.535
$F_{13}(H)$		−0.707	−0.710	−0.716	−0.533	−0.731	−0.550
$F_{14}(H)$		−0.640	−0.649	−0.631	−0.618	−0.471	−0.467

in *para* position to the N-oxide fragment leads to an apparent increase of the N-oxide bond polarity. One conceivable reason for this increase of bond polarity in comparison to the other fluoro 2-NPO derivatives is the direct resonance interaction between the fluorine substituent and the N-oxide group mediated by the ring π-electrons. As is shown in Table 3, the C–F bond length in 2-NPO-4-F is the largest (1.355 Å) within the fluorinated 2-NPOs which

support such way of elucidation. Another possible rationalization of this feature is that the intramolecular dispersion stabilization interaction in all other fluorinated 2-NPOs is more predominant than in 2-NPO-4-F.

While in the monofluorinated 2-NPO derivatives, the variation of the charge density within the ring results from a compromise between the directionality of the nitro group and the fluorine atom, in monofluorinated PO, however, such charge redistribution is dictated only by the *ortho* and *para* directionality of the fluorine atom. Therefore, in all monofluorinated PO derivatives which are shown in Table S9 those ring atoms which are in *ortho* and *para* positions possess higher charge density than all remaining ring atoms.

A comparison between the Mulliken population analysis (MPA) and the natural charge distribution for all pyridine-*N*-oxide derivatives (Tables 5, 6) shows that evident discrepancy exists between the results provided by both charge distribution procedures. For instance, in contrast to the NPA, the MPA suggests negatively charged hydrogen atoms and positive charges on the carbon atoms. Moreover, regardless the significant differences in the evaluation of the charge distribution by both methods, the MPA seems to overestimate the charge depletion and concentration between atoms in a bond. For example in 2-NPO-4-F, the MPA predicts charges of +0.24 on N_1 and −0.78 on O_7, while the NPA suggests +0.04 and −0.52 e$^-$ on these atoms, and thus different degree of bond polarity. By using different wave functions (B3LYP, HF, MP2) and the basis sets (6-311++G(df,pd) and aug-cc-pVDZ) to examine the dependency of both the NPA and Mulliken charge distribution on the level of theory, we found that the MPA provides inconsistent, and in some cases unreasonably fluctuating charge distribution. Most remarkably the MPA at the B3LYP/6-311++G(df,pd) level predicts for the NO_2 group negative charges on nitrogen and positive charges on the oxygen atoms (Table S7) leading to a bond polarity of the type: O^+–N^-–O^+. However, by using the HF/6-311++G(df,pd) method, it provides negative charges on nitrogen as well as on the oxygens (Table S8). This example confirms the previously and repeatedly cited inconsistency of the Mulliken charge distribution and its basis set dependency [37–39].

Since the single atomic charges were not indicative enough to allow for drawing clear conclusions regarding the electronic interplay between the nitro and fluorine substituents and the pyridine-*N*-oxide ring we, therefore, inspired by the work of Zhang et al. [40–42], focused on total charges of the substituent groups and their mutual electronic interaction with the heterocyclic ring. Zhang et al. postulated that there is a relationship between the total Mulliken charges of the NO_2 group (i.e., the sum of the partial charges of the nitrogen and oxygen atoms) and

the molecular stability and structure of a variety of nitrobenzene derivatives (the so-called nitro group charge method [43]). These authors found that the larger the negative charge of the nitro group, Q_{NO_2}, the shorter (the stronger) the R–NO_2 bond and the higher the stability of the nitroaromatic compounds. It is worth to note that Zhang et al. [44, 45] considered the impact sensitivity (which is defined as the height H50 from where a given weight falling upon the compound gives 50 % probability on initiating an explosion) as a measure for the stability of energetic materials. We extended this concept and considered the total charges of the ring atoms and each of the ring substituents and investigated whether these total charges can provide useful and direct indications of any alterations of the structural parameters in the substituted pyridine-*N*-oxides that we discussed above.

The total natural charges of the ring, Q_{ring}, the nitro group, Q_{NO_2}, and the methyl group, Q_{methyl}, as obtained from B3LYP/aug-cc-pVDZ are listed in Table 7. From this table, it is evident that the nitration of the PO in *ortho* position results in a reduction of the natural charges of the ring by 0.353 e$^-$ due to the strong electron withdrawal ability of the nitro group. Adding a fluorine substituent next to the nitro group, 2-NPO-3-F, leads to an additional loss of the ring charges by 0.533 e$^-$, and thus the net charge of the ring becomes positive. It seems that the variation of the

Table 7 Total natural charges of the pyridine ring Q_{ring}, the nitro group Q_{NO_2}, the methyl group Q_{CH_3} in pyridine-*N*-oxide (PO), 2-nitropyridine-*N*-oxide (2-NPO) in addition to 3-methyl-2-nitropyridine-*N*-oxide (3-methyl-2-NPO), 5-methyl-2-nitropyridine-*N*-oxide (5-methyl-2-NPO) and their 6-fluoro derivatives

	Q_{ring}	Q_{NO_2}	Q_{CH_3}	R_{C-NO_2}
PO	−0.681			
2-NPO	−0.328	−0.200		1.471
2-NPO-3-F	0.205	−0.157		1.474
2-NPO-4-F	0.224	−0.169		1.476
2-NPO-5-F	0.212	−0.214		1.467
2-NPO-6-F	0.197	−0.170		1.477
2-NPO-F4	1.842	−0.138		1.476
3-F-PO	−0.142			
4-F-PO	−0.123			
6-F-PO	−0.152			
F4-PO	1.501			
3-Methyl-2-NPO	−0.136	−0.181	0.087	1.477
5-Methyl-2-NPO	−0.136	−0.221	0.077	1.467
3-Methyl-6-F-2-NPO	0.391	−0.174	0.088	1.478
5-Methyl-6-F-2-NPO	0.398	−0.206	0.087	1.469
2-Methyl-6-F-PO	0.041		0.077	
2,6-Difluoro-PO	0.375			

R_{C-NO_2} is the C–NO_2 bond length in Å (B3LYP/aug-cc-pVDZ was used)

fluorine position on the ring does not markedly affect the Q_{ring} value. The considerable increase of the positive charges of the ring of $Q_{ring} = +1.84$ e$^-$ in 2-NPO-F4 was obviously expected due to the appreciable electron withdrawal by the four fluorine atoms. Such kind of consideration is also valid for the tetrafluoro PO.

Interestingly, the fluorination of the PO ring in *meta* position (3-F-PO) leads to a loss of ring charges of 0.54 e$^-$, which is comparable to the reduction of ring charge (0.53 e$^-$) on going from 2-NPO to 2-NPO-3-F. Table 7 shows that substantial variation of the Q_{ring} value by the nitration or fluorination of PO in *ortho* position to the N-oxide fragment occurs. It is also worth noting that the largest loss of ring charges within the monofluorinated derivatives occurs on going from PO to 2-NPO-4-F, where ΔQ_{ring} is 0.91 e$^-$, and the smallest loss of charges emerges upon moving from PO to 2-NPO-6-F, where ΔQ_{ring} amounts to 0.88 e$^-$. This is because of the fluorine hyperconjugative effect and the increase of the charge density in *ortho* position and the higher electronegativity of the oxygen atom. From Table 7, it can be seen that the fluorination of PO leads to a significant loss of ring charges ranging from 0.558 e$^-$ in the case of 4-F-PO to 0.529 e$^-$ in 6-F-PO. The nitration of PO in *ortho* position results in a decrease of the ring charges by only 0.353 e$^-$. Obviously the insertion of four fluorine substituents to PO and 2-NPO results in a considerable loss of ring charges of $\Delta Q_{ring} = 2.18$ e$^-$ and 2.17 e$^-$, respectively. This result is somehow intriguing because the alteration of Q_{ring} upon fluorination is almost the same in both cases regardless the nitration of PO in *ortho* position.

The substitution of the methyl group in *ortho* and *para* positions to the nitro group in 2-NPO provides Q_{ring} values which reflect to some extent the hyperconjugative interaction of the methyl group. A comparison between the Q_{ring} values of 2-NPO-3-F and 3-methyl-2-NPO reveals that the substitution of the fluorine atom by the methyl group in *ortho* position to the nitro group increases the ring charge density by 0.34 e$^-$. Similarly, the substitution of fluorine in 2-NPO-5-F by the electron donating CH$_3$ group (which is in *para* position to the nitro group) raises Q_{ring} by 0.35 e$^-$. As Table 7 also shows the loss of ring charge of 0.53 e$^-$ upon the fluorination of 3- and 5-methyl-2-NPO in *ortho* position to the N-oxide group is significantly large. Remarkably is that the methyl group seems to donate approximately the same amount of natural charges into the heteroaromatic system regardless the nitration in position 2 and fluorination in various positions on the ring which is reflected by the similar Q_{CH_3} values in Table 7.

In addition, Table 7 shows that, except for few exemptions, the more the NO$_2$ group is negatively charged the shorter, and thus the stronger, the C–NO$_2$ bond is. Such

finding is in agreement with the postulated correlation between the negative charges of the nitro group, Q_{NO_2}, and the C–NO$_2$ bond strength [40–42]. Following this relationship, Table 7 demonstrates that 5-methyl-2-NPO is the most stable and 2-NPO-F4 is the least stable compound. Consequently, the latter compound possesses in comparison to the former one larger impact sensitivity (smaller H50 value). Perhaps of interest to note that in contrast to the findings of Zhang et al. [40] we found that using the Q_{NO_2} Mulliken charges (Table S10) instead of the natural charges (Table 7) for the nitropyridine-N-oxide compounds leads to an apparent disagreement with this Q_{NO_2}/R_{NO_2} relationship. So for instance the largest Q_{NO_2} Mulliken charge is −0.734 for 3-methyl-2-NPO and the smallest value is −0.634 for 2-NPO-5-F, but the C–NO$_2$ bond lengths are 1.477 and 1.467 Å, respectively, which is clearly inconsistent with the Zhang relationship. Accordingly, we recommend using the natural charges instead of the Mulliken charges by applying this concept.

It should be pointed out that the group charges, Q, do not provide direct indications of directionality of substitution on the heteroaromatic ring, since different substituents have different directing effects due to their inductive or resonance interactions and their relative positions to each other. All these factors can lead to additive or opposing subtracting effects which dictate the reactivity of a certain position on the ring and its readiness for electrophilic or nucleophilic attack. Aside from that the proximity of the positions of the substituents can give rise to dipolar, Pauli exchange, or intramolecular dispersion interactions.

The NO$_2$ torsional motion and potential functions

In order to better understand the dependency of the potential energy on the variation of the molecular geometry of the 2-NPOs under study, we investigated the potential energy function of the internal rotation of the nitro group about the N$_8$–C$_2$ bond. For this purpose, we carried out relaxed potential energy surface scans by the variation of the dihedral angle $\gamma = $ O$_9$–N$_8$–C$_2$–N$_1$ in intervals $+10°$ between $0°$ and $180°$, and by applying different levels of model chemistries. One main target of such investigations was to explore the influence of (a) the variation of the applied wave function, (b) the level of the chosen basis set, (c) the augmentation of the basis sets with diffuse functions, and (d) the substitution of hydrogens by a fluorine atom at various ring positions on the torsional motion of the NO$_2$ group about the C$_2$–N$_8$ axis and the potential function describing it.

As is clearly evident from all the potential curves describing the torsional motion of the NO$_2$ group and which are shown in this work the variation of the basis set

(and in some instances the alteration of the wave function as well) has tremendous impact on the profile and the barrier height of the potential function. It is beyond the scope of this work to present the whole variety of the different kinds of the dependency of the torsional potential of the nitro group on the applied basis set for all the investigated compounds in this study. Therefore, only a selection of these potential functions is displayed.

This significant dependency of the multiplicity and form of the torsional potential on the augmentation of the basis set with diffuse functions is remarkable. The computational results which we obtained from this study clearly demonstrate that particular caution should be exercised when investigating energy minima on the potential energy hypersurface by performing quantum mechanical calculations and applying various basis sets (and wave functions) at different levels of theory.

2-NPO

Aside from the anticipated structural consequences of the application of different levels of model chemistry, we observed that, regardless the computational methods, the inclusion of diffuse functions in the basis sets have the most substantial influence on the predicted torsional potential function of the nitro group.

Inspection of Fig. 3 unveils that the augmentation of the 6-31G(df,pd) basis set with diffuse functions on all atoms shows a marked effect on the form of the torsional potential function (Fig. 3e, f). In the case of the Hartree–Fock wave function, the inclusion of the diffuse functions changes the torsional potential function from a double-minimum potential with very low rotational barrier of 0.15 kcal mol^{-1} at $\gamma = 90°$ to a flat single minimum potential and increases the potential barrier at $\gamma = 0°$ by 1.1 kcal mol^{-1}. The addition of diffuse functions leads in the case of the B3LYP and MP2 wave functions to lowering of the potential barriers at $90°$ by 1.2 and 0.5 kcal mol^{-1} and elevates the barrier at $0°$ by 0.7 and 1.5 kcal mol^{-1}, respectively (Fig. 3e, f).

To examine the effect of using larger basis set on the form of the rotational potential function we employed the 6-311 basis set. Figure 3a shows that by using the HF, B3LYP, and MP2 wave functions in combination with this triple-zeta basis set augmented with polarization functions the torsional motion of the nitro group describes a double-minimum potential with variable barrier heights on the potential energy surface, i.e., first maximum at 2.9, 1.1, and 2.5 kcal mol^{-1} and a second maximum at 0.1, 0.9, and 0.5 kcal mol^{-1} as predicted by HF, B3LYP, and MP2, respectively. Furthermore, a shift of the energy minima occurs upon moving from HF to B3LYP and MP2 wave functions ($\gamma = 68°$, $40°$, and $54°$, respectively). The

extension of the triple-zeta basis set by diffuse function on all atoms leads interestingly to an evident increase of the potential barrier of the first maximum ($\gamma = 0°$) and to a slight decrease of the barrier of the second maximum ($\gamma = 90°$) regardless which computational method is used (Fig. 3b). This increase amounts to 0.8, 0.6, and 1.0 kcal mol^{-1} as obtained from applying the HF, B3LYP, and MP2 methods.

From Fig. 3c, it can be seen that the application of the same wave functions in combination with Dunning correlation consistent basis set cc-pVDZ provides double-minimum potential curves but with significantly lower potential barriers. Interestingly, the application of cc-pVTZ basis set in combination with HF has produced single minimum potential function at $\gamma = 90°$ and high potential barrier of 3.7 kcal mol^{-1}. The combination of this basis set with MP2 and B3LYP wave functions suggested a double-minimum potential at $\gamma = 56°$ and $124°$ (Fig. S1). The addition of diffuse functions to the Dunning double-zeta basis set produces the most conspicuous alteration of the shape of the torsional potential energy functions. From Fig. 3d, it is evident that this augmentation of the basis set leads to the appearance of a single minimum potential at $90°$ in the case of the HF wave function (instead of double-minimum potential without augmentation) and a broad flat potential well over the range of $\gamma = 50°–140°$ occurs when the MP2 and B3LYP wave functions are used. Many attempts have been undertaken by using different starting values for the torsional angle, γ, to find the global potential energy minimum for 2-NPO but in summary we obtained optimized values for γ ranging from $83°$ to $93°$ with almost negligible differences of the total energy and very low positive frequencies.

Fluoro derivatives

As it was alluded to above, one of the main objectives of this work is to explore the effect of the variation of the model chemistries and the fluorine substitution on the form of the torsional potential of the nitro group and the potential barriers. Accordingly, we analyzed the torsional potential of the NO_2 group for 2-NPO-x-F (where $x = 3, 4, 5, 6$, the position of the F substitution on the ring) and 2-NPO-F4 and compared these potentials with that of 2-NPO.

Effect of the selected wave function

This study has generally demonstrated that the employment of different wave functions leads in most cases to a minor shift of the energy minima, but results in a considerable inconsistent alteration of the barrier heights for internal rotation of the NO_2 group. For instance, the scan analysis
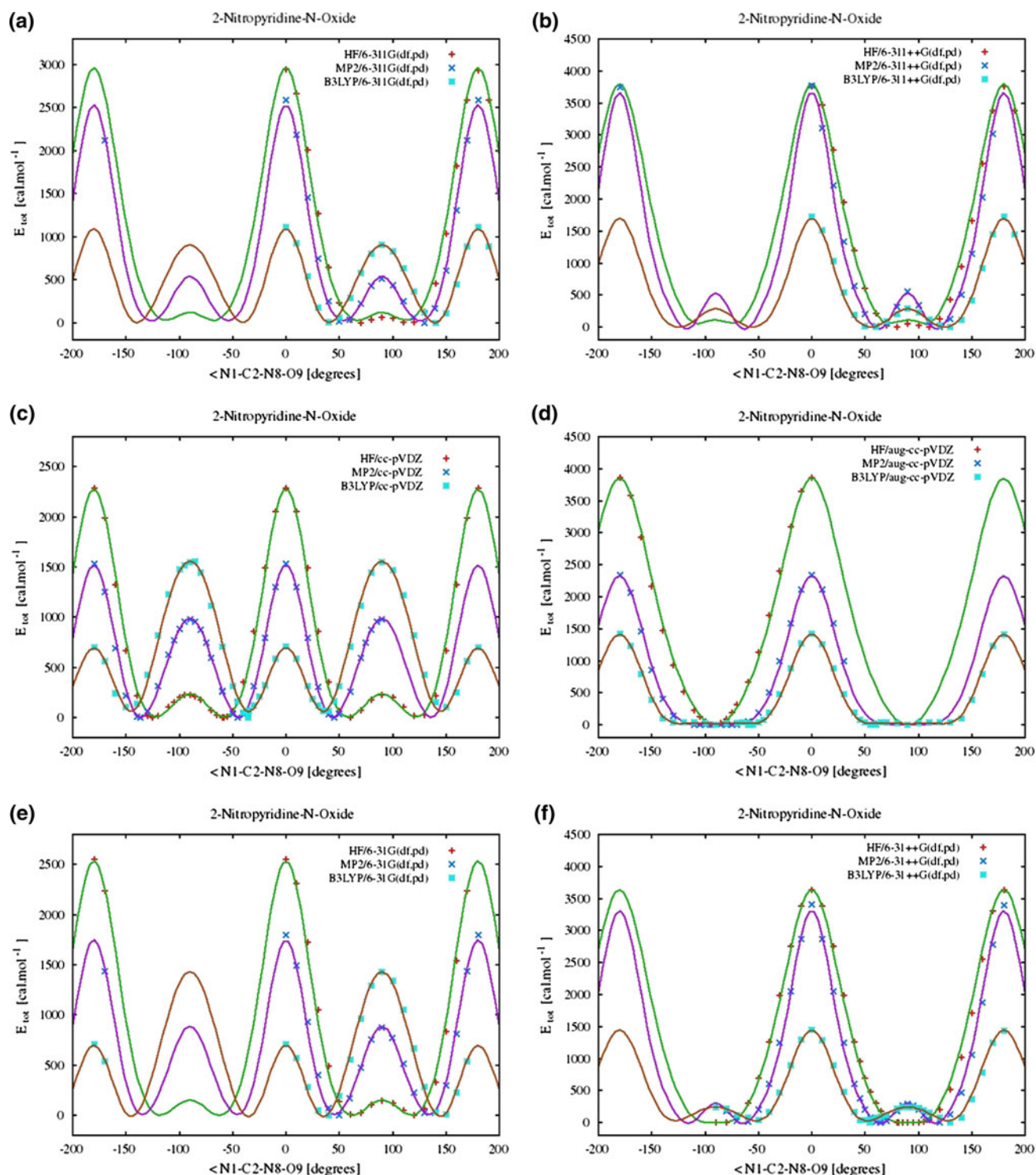
Fig. 3 NO_2 torsional potential for 2-NPO and its dependency on the level of theory and the augmentation with diffuse functions (γ is the dihedral angle N_1–C_2–N_8–O)

of the internal rotation of the nitro group in 2-NPO by using the HF and MP2 methods in combination with the cc-pVDZ basis set (Fig. 3c) indicates that the application of different wave functions has almost no effect on the trend

of the potential function. Nevertheless, the barrier heights at $\gamma = 0°$ and $\gamma = 90°$ drop from 2.27 to 0.23 and from 1.52 to 0.99 kcal mol^{-1} upon using the HF instead of the MP2 wave function. Employing the B3LYP wave function,

however, leads to an inversion of the barrier heights at $\gamma =$ 0° and $\gamma = $ 90° which means that in contrast to above mentioned methods the density functional method predicts a barrier at $\gamma = $ 90° which is by 0.9 kcal mol^{-1} higher than that at $\gamma = $ 0°. Likewise, the application of the same wave functions in combination with the Pople double-zeta basis set for scanning the NO_2 rotational potential function provides analogous trend. Interestingly, similar dependency of the NO_2 torsional potential function on the applied wave function was obtained for various fluorinated 2-NPOs whose NO_2 torsional potential functions exhibit two distinctive energy maxima at $\gamma = $ 0° and $\gamma = $ 90°, i.e., 2-NPO-4-F, 2-NPO-5-F, and 2-NPO-6-F (Figs. 4, 5). The application of the MP2/cc-pVDZ computational method predicts potential barriers for the NO_2 internal rotation in these compounds (Fig. 4c, e, 5a) of 1.22, 1.41, 1.39 kcal mol^{-1} at $\gamma = $ 0° and 1.10, 1.12, and 1.11 kcal mol^{-1} at $\gamma = $ 90°. For comparison, the B3LYP/cc-pVDZ method suggests barrier heights of 0.49, 0.51, and 0.66 kcal mol^{-1} at $\gamma = $ 0° and 1.45, 1.88, and 1.42 kcal mol^{-1} at $\gamma = $ 90°. In conclusion, the barrier heights at $\gamma = $ 0° and $\gamma = $ 90° undergo an inversion upon the alteration of the wave function (and a slight shift of the potential minima) which parallels the behavior of the potential barriers in 2-NPO. It remains to point out that using Pople's triple-zeta basis set along with the MP2 and B3LYP wave functions for scanning the NO_2 rotational potential barriers has shown that only in the case of 2-NPO-5-F (not in 2-NPO-4-F and 2-NPO-6-F) such an inversion of the barrier heights occurs (Fig. 4e).

Effect of the implementation of diffuse functions

From our calculations, it has become apparent that generally an increase of the barriers for the NO_2 torsional potential at $\gamma = $ 0° by roughly 0.5–2.3 kcal mol^{-1} occurs on the augmentation of any of the basis sets, we used with diffuse functions regardless the computational method that has been employed. Figures 4 and 5 compare the potential energy functions resulting from augmentation of the 6-311 and cc-pVDZ basis sets by diffuse functions on all atoms with those which were obtained from non-augmented basis sets.

2-NPO-3-F

Figure 4a shows that for 2-NPO-3-F similar profiles of the potential functions for the internal rotation of the NO_2 group were obtained by using the MP2 and B3LYP wave functions in combination with Pople triple-zeta and Dunning double-zeta basis sets. Utilizing these basis sets has produced a double-minimum potential with a hump-like very low potential barrier between the two minima of

approximately 0.2 kcal mol^{-1}. Augmenting the cc-pVDZ basis set with diffuse functions leads to a single minimum potential at $\gamma = $ 90° for both wave functions (Fig. 4b). The potential barriers at $\gamma = $ 0° by employing the density functional method in combination with the cc-pVDZ and aug-cc-pVDZ basis sets are by 1.1 and 1.5 kcal mol^{-1} lower than predicted by the MP2 method in combination with these basis sets. Further, the augmentation of the 6-311G(df, pd) basis set with diffuse functions has led to an increase of the potential barrier at $\gamma = $ 0° by 1.2 and 1.3 kcal mol^{-1} by applying the MP2 and B3LYP wave functions, respectively.

2-NPO-4-F

As is evident from Fig. 4c, the application of B3LYP and MP2 wave functions and the cc-pVDZ basis set predicts a double-minimum potential at $\gamma = $ 33° and 147° for the B3LYP and at $\gamma = $ 42° and 138° for the MP2 wave function. The potential barriers at $\gamma = $ 0° and $\gamma = $ 90° amount to 0.49 and 1.45 kcal mol^{-1} as produced by the B3LYP/cc-pVDZ model chemistry and to 1.22 and 1.10 kcal mol^{-1} as obtained from the MP2/cc-pVDZ method. Augmenting this basis set with diffuse functions drastically changes the profile of the torsional potential function of the nitro group and provides for B3LYP and MP2 a shallow single minimum potential ranging from $\gamma = $ 60° to $\gamma = $ 120° (Fig. 4d). The height of the potential barrier at $\gamma = $ 0° rises to 1.27 and 1.93 kcal mol^{-1} for the B3LYP and MP2 wave functions, respectively. These results are at variance with those which were obtained after the addition of diffuse functions to the 6-311G(df,pd) basis set. In this case, the double-minimum potential remains unchanged but the potential barrier at $\gamma = $ 0° increases by 0.6 and 1.1 kcal mol^{-1} by using B3LYP and MP2, respectively, and the barrier height at $\gamma = $ 90° decreases by 0.6 kcal mol^{-1} when using B3LYP, and remains almost unchanged by applying the MP2 wave function.

2-NPO-5-F

A large impact on the barrier heights emerges upon the addition of diffuse functions to the Dunning cc-pVDZ basis set (Fig. 4f). While the increase of the NO_2 torsional barrier at $\gamma = $ 0° amounts to 0.5 and 0.7 kcal mol^{-1} by using the B3LYP and MP2 wave functions, respectively, the maximum at $\gamma = $ 90° decreases by 1.6 and 1.1 kcal mol^{-1}. This augmentation with diffuse functions has also lead to a shift of the positions of the potential minima from 31° to 46° by using B3LYP and from 42° to 65° by choosing MP2 wave function. For comparison, the addition of diffuse functions to the 6-311G(df,pd) basis set resulted in an increase of the

potential barrier at $\gamma = 0°$ by 0.5 and 1.0 kcal mol^{-1} by applying the B3LYP and MP2 wave functions, respectively, whereas the barrier at $\gamma = 90°$ lowers by 0.7 kcal

mol^{-1} in the case of the B3LYP method and remains almost unaffected when the MP2 method was used (Fig. 4f).
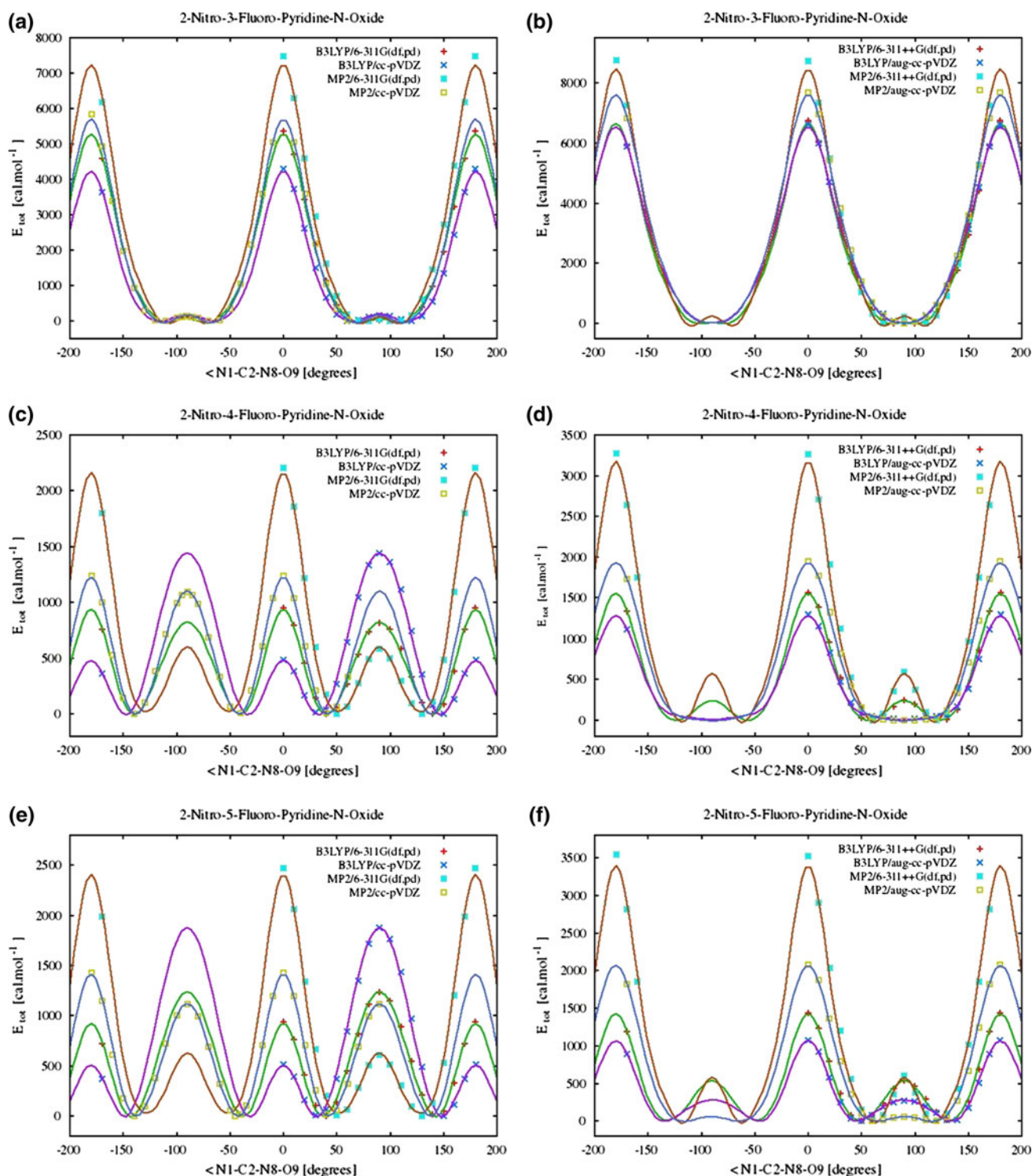

Fig. 4 NO$_2$ torsional potential for 2-NPO-3-F, 2-NPO-4-F, and 2-NPO-5-F and its dependency on the level of theory and the augmentation with diffuse functions (γ is the dihedral angle N$_1$–C$_2$–N$_8$–O)
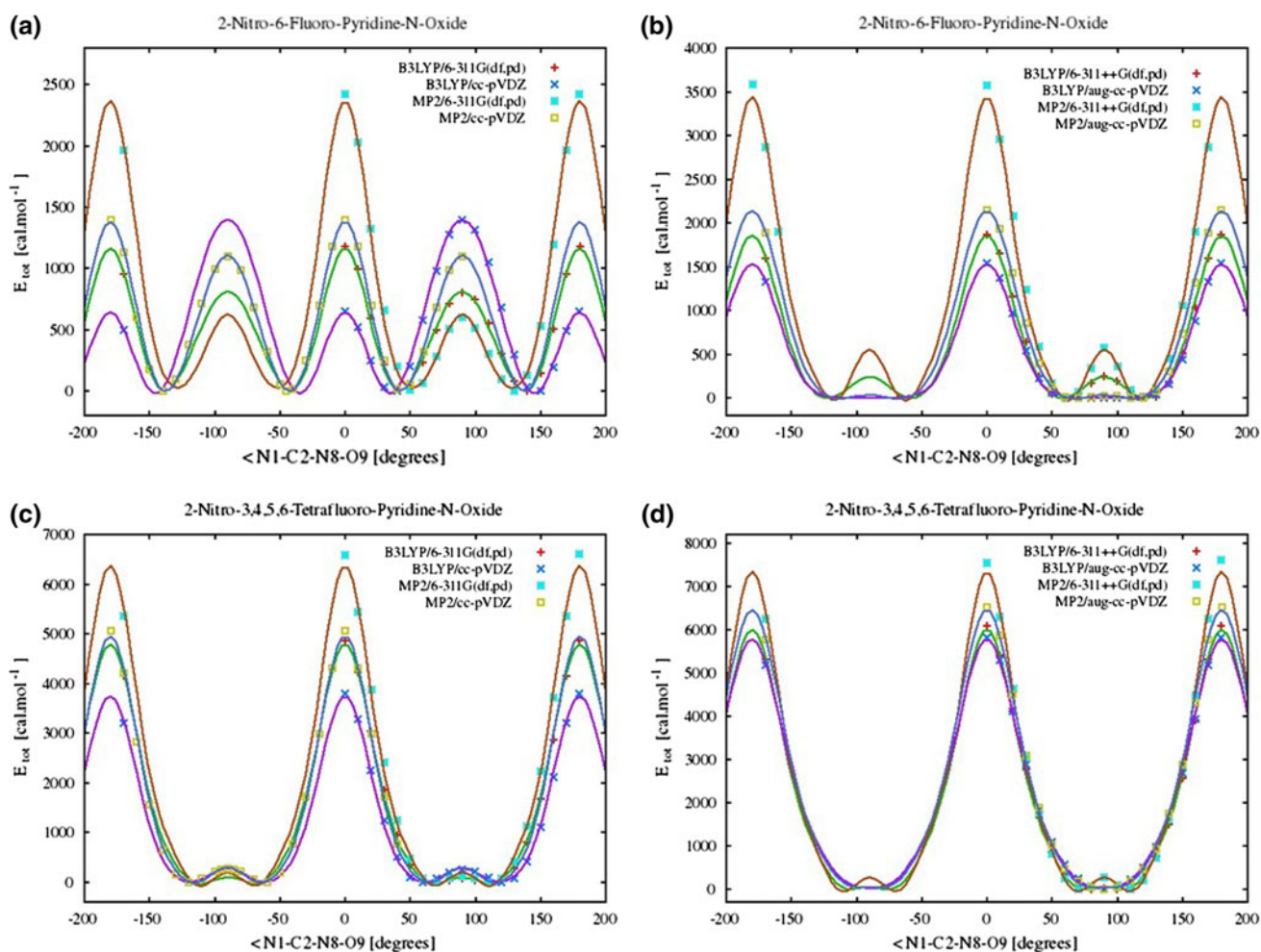
Fig. 5 NO₂ torsional potential for 2-NPO-6-F and 2-NPO-F4 and its dependency on the level of theory and the augmentation with diffuse functions (γ is the dihedral angle N_1–C_2–N_8–O)

2-NPO-6-F

As Fig. 5b shows the inclusion of diffuse functions into the cc-pVDZ basis set leads to a transition from a double-minimum torsional potential to a flat single minimum potential ranging from $\gamma = 60°$ to $120°$ regardless the computational method has been used. This behavior resembles the behavior of the torsional potentials in 2-NPO and 2-NPO-4-F. Due to this extension of the basis set, the potential barrier at a torsional angle of $0°$ increases by 0.8 and 0.7 kcal mol^{-1} by applying B3LYP and MP2, respectively. Also in analogy to 2-NPO and 2-NPO-4-F the augmentation of the 6-311G(df,pd) basis set by diffuse functions does not significantly affect the profile of the double-minimum torsional potential except the positions of the minima shift to a slightly larger torsional angle ($\Delta\gamma = 16°$ for B3LYP and $11°$ for MP2) and the barrier heights at $\gamma = 0°$ are lower by 0.7 and 1.1 kcal mol^{-1} and at $\gamma = 90°$ by 0.6 and 0.02 kcal mol^{-1} for B3LYP and MP2, respectively.

2-NPO-F4

While the B3LYP and MP2 wave functions in combination with the basis sets cc-pVDZ and 6-311G(df,pd) (Fig. 5c) yield similar double-minimum torsional potential functions with a very low torsional barrier (<0.3 kcal mol^{-1}) at $\gamma = 90°$, the implementation of diffuse functions have different impact on these potential functions. The augmented Dunning correlation consistent basis set produces with B3LYP and MP2 a single minimum potential at $\gamma = 90°$ and an increase of the potential barrier at $\gamma = 0°$ by 2.0 and 1.5 kcal mol^{-1}, respectively, demonstrating that both model chemistries describe the intramolecular interactions in 2-NPO-F4 equally well. Upon the addition of diffuse functions to the 6-311G(df,pd) basis set, the double-minimum potential with a quite low barrier at $\gamma = 90°$ (<0.3 kcal.mol^{-1}) for internal rotation of the NO₂ group remains unchanged by applying both wave functions. Nevertheless, the potential barrier at $\gamma = 0°$ rises by ~ 1.0 and 1.2 kcal mol^{-1} (Fig. 5d).

Interesting features emerge from the comparison of the potential functions in 2-NPO, 2-NPO-6-F, and 2-NPO-3-F as produced by MP2/aug-cc-pVDZ. For 2-NPO and 2-NPO-6-F, a flat broad minimum ranging from $\gamma = 60°$ to $\gamma = 120°$ was obtained. However, in the case of 2-NPO-3-F, the potential function shows a distinctive minimum at $\gamma = 90°$ (Fig. 4b). From this comparison, it can be concluded that the nitro group in both instances, where either the fluorine substituent is absent (2-NPO) or is not in *ortho* position to the nitro group (2-NPO-6-F), this group performs a large amplitude motion, which is manifested by the flat broad minimum as Figs. 3d and 5b demonstrate. On the other hand, the seemingly attractive interaction between the nitro group and the fluorine atom in 2-NPO-3-F suppresses such large amplitude motion which is evident from the sharp potential minimum at $\gamma = 90°$.

Assuming that steric interactions and intramolecular hydrogen bonding do not play a prominent role by the determination of rotational barriers in the investigated 2-NPOs, it can be postulated that the shorter the $C–NO_2$ bond (the larger the bond strength), the higher is the barrier for internal rotation of the nitro group. Chen et al. [46, 47] and others [48] have found that such correlation is excellently applicable to a variety of aromatic nitro compounds. This correlation seems to be invalid for the series of heteroaromatics which we presented in this work. From Table 3, it is evident that the $C–NO_2$ bond length varies only marginally within the fluoronitropyridine-N-oxides, but on the other side, the potential barriers for the NO_2 internal rotation fluctuate over a wide scale of potential energy no matter which computational method is used. For instance, by applying MP2/aug-cc-pVDZ the potential barrier at $\gamma = 0°$ varies between 1.9 kcal mol^{-1} for 2-NPO-4-F and 7.6 kcal mol^{-1} for 2-NPO-3-F (Fig. 4b, d). Further, MP2/6-311++G(df,pd) predicts a variation of this barriers ranging from 3.2 kcal mol^{-1} in 2-NPO-4-F to 8.5 kcal mol^{-1} in 2-NPO-3-F, whereas the alteration of the $C–NO_2$ bond length within these fluorinated 2-NPOs amounts only to ±0.001 Å. One conceivable interpretation of this striking behavior is that the barrier heights for the internal rotation of the nitro group in the fluorinated heterocyclic series depends on the proximity or remoteness of the fluorine substituent to the nitro or the N-oxide fragment. These barriers are predominantly governed either by attractive intramolecular fluorine–oxygen dispersion interaction or O···H hydrogen bonding but less by mesomeric or hyperconjugative interactions and an increase of the $C–NO_2$ bond strength.

It is worth to make a general note which is valid for all structural results and NO_2 torsional potential energy functions which were obtained by applying density functional wave function and small or medium basis sets: it is well known that the DFT potentials miss or underestimate (depending on the quality of the exchange–correlation functionals) the long-range dispersion and overlap or medium dispersion. However, the different rotamers represented by the energy minima on the potential energy surface for all nitropyridine-N-oxides throughout this study are mostly stabilized by intermediate- or long-range interactions on the torsional potential energy surface.

Grimme et al. [31] have very recently pointed out that the inclusion of dispersion corrections into the standard density functional is essential, particularly when dealing with large and medium size molecules containing electron-rich and polarizable functional groups. In addition, the application of small to medium basis sets (even in combination with second-order perturbation wave function) are afflicted by a basis set superposition error (BSSE) [49]. The missing dispersion correlations and BSSE by using smaller size basis sets like 6-31 and 6-311 with single polarization functions and limited augmentation with diffuse function may substantially obscure the search of minima on the potential energy surface, e.g., hiding minima or leading to artificial minima [50].

By using basis sets augmented with polarization functions of higher angular momentum and diffuse functions on all atoms, we ensured that the computed structural parameters and potential functions in this work do not suffer from BSSE. It is important to take into consideration that the potential function and the magnitude of the barriers for internal rotation of the nitro group also comprise the contributions of the ring deformation energy and deviation from planarity during the NO_2 rotation about the $C–NO_2$ axis. Moreover, essentially the potential energy function does not include entropic effects. Consequently, an energy minimum in the potential function corresponds to a minimum of the free energy rather than to the equilibrium, or the most probable state.

Effect of the fluorine substitution

From all the above-described behavior of the torsional potential of the NO_2 group on the potential energy surface is evident that, beside the significant influence of the basis sets on the barrier height for internal rotation of this group, the fluorine substitution has profound effect on these potential barriers and the energetic preference of rotamers. For instance, a comparison between the profiles of the potential function for 2-NPO and 2-NPO-3-F as predicted by the MP2/cc-pVDZ method reveals that the potential barrier at $\gamma = 0°$ grows noticeably by 4.2 kcal mol^{-1} and the barrier at $\gamma = 90°$ lowers by 0.8 kcal mol^{-1}. By using the 6-311G(df,pd) basis set, the barrier at $\gamma = 0°$ and $\gamma = 90°$ increases by 4.8 and decreases by 0.3 kcal mol^{-1}, respectively. Adding diffuse functions to these basis sets leads to rather higher potential barrier at $\gamma = 0°$ (Figs. 3b, d, 4b).

Similar decisive effect of the fluorination on the potential energy barriers is apparent from the consideration of 2-NPO-F4. The tetrafluorination of 2-NPO elevates the barrier for internal rotation of the NO_2 moiety at $\gamma = 0°$ by 3.5 kcal mol^{-1} and reduces this barrier at $\gamma = 90°$ by 0.7 kcal mol^{-1} when MP2/cc-pVDZ was used. Applying MP2/6-311G(df,pd) provided 3.9 and 0.3 kcal mol^{-1}, respectively (Fig. 5c).

In this regard, it should be pointed out that in 2-NPO-4-F and 2-NPO-5-F, where the fluorine substituent is at remote positions to the NO_2 and N-oxide fragments, the effect of the fluorination on the potential barriers is less accentuated, since electrostatic and Pauli exchange repulsive interactions (steric effects) play minor role in these compounds.

NBO analysis

To gain more insight into the reasons leading to the departure of the nitro group from the co-planarity with the ring and the alteration of the bond distances and angles within the explored 2-NPOs, we carried out natural bond orbital (NBO) analysis [51–55] on the optimized structures of these compounds employing the B3LYP and HF wave functions in combination with the aug-cc-pVDZ, and 6-311++G(df,pd) basis sets.

Further reasons for utilizing this NBO scheme were: (i) to obtain more supporting details about the nature of electronic interactions between the substituents and the ring skeleton and the mutual interactions between the substituents, (ii) to investigate more thoroughly whether the torsional potential function of the nitro group is governed by negative and/or positive hyperconjugative charge delocalization interactions between filled Lewis orbitals and vacant NBOs (bond–antibond interactions) or by steric repulsive interactions involving Pauli exchange repulsion. For more profound rationalization of the latter interaction, we carried out an NBO deletion analysis by applying the NOSTAR (deletion of all antibonding and Rydberg orbitals), NOVIC, and NOGEM (deletion of all vicinal and all geminal bond–antibond interactions, respectively) algorithms. Furthermore, the most relevant specific donor/acceptor interactions have been switched off to obtain details about their quantitative contributions to the total electronic delocalization energy of the studied 2-NPOs. We also analyzed the delocalization energies as estimated by the second-order perturbation theory (SOPT) in the NBO space. These energy values reflect the extent of charge delocalization from a Lewis- to non-Lewis (bond–antibond) NBOs and, thus, indicate the strength of bond–antibond hyperconjugative interactions between NBOs.

In the following, only some crucial results of the NBO analysis will be scrutinized and interpreted. Perhaps the most essential features which have been provided by this

analysis were the demonstration of the prominent role of the lone pair electrons by the determination of the structure and rotamers stability of the fluorinated 2-NPOs under consideration and thus of their potential energy function. In this context, it is worth to note that in all these compounds, the lone electron pair orbitals ($n_{\pi2}$) on the oxygen atoms in the N-oxide and NO_2 groups have the lowest orbital charge population and, therefore, the most significant deviation from the idealized Lewis occupancy. For instance, the $n_{\pi2}$ orbitals on the N-oxide oxygen, O_7, are occupied by 1.62, 1.65, 1.58, 1.63, and 1.63 electrons (at the B3LYP/6-311++G(df,pd) level) in 2-NPO-3-F, 2-NPO-4-F, 2-NPO-5-F, 2-NPO-6-F, and 2-NPO-F4, respectively, which is way off from the Lewis occupancy. This appreciable loss of electronic charges is mainly due to delocalization of electrons from these occupied orbitals to the vacant non-Lewis antibond orbital $\pi^*_{N_1-C_6}$. As is apparent from Table 8, the SOPT approach indicates that the perturbation energy for this charge delocalization at the B3LYP/6-311++G(df,pd) level is considerably large and amounts to 58.5, 62.2, 54.0, 69.8, 66.0, and 70.2 kcal mol^{-1} for 2-NPO, 2-NPO-3-F, 2-NPO-4-F, 2-NPO-5-F, 2-NPO-6-F, and 2-NPO-F4, respectively. For comparison, the HF/6-311++G(df,pf) method provides stabilization energy values for this $(n_{\pi2})_{O_7} \rightarrow \pi^*_{N_1-C_6}$ charge transfer of 69.5, 79.0, 59.6, 85.4, 63.7, and 72.6 kcal mol^{-1} (Table S11). It is also noticeable that in 2-NPO, 2-NPO-3-F, 2-NPO-4-F, and 2-NPO-5-F, the donor–acceptor hyperconjugative interaction $(n_{\pi1})_{O_7} \rightarrow \sigma^*_{N1-C2}$ is energetically more favored than the $(n_{\pi1})_{O_7} \rightarrow \sigma^*_{N1-C6}$ charge transfer. However, in 2-NPO-6-F and 2-NPO-F4 where the fluorine substituent is adjacent to the N-oxide fragment, this preferability is reversed.

Obviously, due to resonance stabilization within the nitro group, the donor–acceptor $(n_{\pi2})_{O_{10}} \rightarrow \pi^*_{N8-O9}$ shows the largest stabilization energy. It is also worth to point out that the delocalization energy for the $(n_{\pi1})_{O_9} \rightarrow \sigma^*_{N8-O10}$ and $(n_{\pi1})_{O_{10}} \rightarrow \sigma^*_{N8-O9}$ charge transfer interactions are different by approximately 1.0 kcal mol^{-1} in 2-NPO-5-F and 2-NPO-6-F. One possible explanation for this disparity is the deviation of the NO_2 group from co-planarity with the heteroaromatic ring and the −sc/ac arrangement of the N=O bonds. (Table 3). Beside the various donor–acceptor π–π^* resonance delocalization interactions within the heteroaromatic ring, the interaction between the fluorine lone electron pairs and the different non-Lewis orbitals plays a crucial role by the donor/acceptor stabilization of the fluorinated 2-NPOs under consideration.

Table 8 indicates that the most significant fluorine lone pair hyperconjugative interaction occurs between the $(n_{\pi2})_F$ orbitals and the antibonding π^* orbitals of the adjacent ring C=C bonds. The $E(2)$ stabilization energy for this donor–acceptor interaction amounts to 21.9, 22.1, and 20.2 kcal

Table 8 Some results of the NBO analysis of donor–acceptor interactions and stabilization energies (E2) for 2-nitropyridine-N-oxide (2-NPO) and its fluorinated derivatives as estimated by the second-order perturbative scheme using the B3LYP/6-311++G(df,pd) method

Donor orbital	Acceptor orbital	2-NPO	2-NPO-3-F	2-NPO-4-F	2-NPO-5-F	2-NPO-6-F	2-NPO-F4
$\pi_{N_1-C_6}$	$\pi^*_{C_2-C_3}$	18.0	17.5	22.8	15.7	18.1	17.5
$\pi_{N_1-C_6}$	$\pi^*_{C_4-C_5}$	11.9	13.1	10.8	13.7	10.9	11.7
$\pi_{C_2-C_3}$	$\pi^*_{N_1-C_6}$	14.5	15.1	15.0	16.4	14.1	13.9
$\pi_{C_2-C_3}$	$\pi^*_{C_4-C_5}$	16.0	14.6	19.4	14.5	16.9	16.2
$\pi_{C_2-C_3}$	$\pi^*_{N_8-O_9}$				12.3	8.4	
$\pi_{C_4-C_5}$	$\pi^*_{N_1-C_6}$	33.6	30.1	33.6	30.0	37.8	30.1
$\pi_{C_4-C_5}$	$\pi^*_{C_2-C_3}$	24.1	27.1	21.4	25.7	22.4	21.7
$\pi_{N_8-O_9}$	$(n_{\pi2})_{O_{10}}$	14.0	13.7	14.1	12.0	12.2	14.0
$(n_{\pi1})_{O_7}$	$\sigma^*_{N_1-C_2}$	11.5	11.5	9.7	12.2	11.3	10.9
$(n_{\pi1})_{O_7}$	$\sigma^*_{N_1-C_6}$	8.8	9.0	8.3	9.5	11.9	12.0
$(n_{\pi2})_{O_7}$	$\pi^*_{N_1-C_6}$	58.5	62.2	54.0	69.8	66.0	70.2
$(n_\sigma)_{O_9}$	$(Ry*)_{N_8}$	5.6	5.3	6.1	5.5	5.4	5.4
$(n_{\pi1})_{O_9}$	$\sigma^*_{C_2-N_8}$	14.1	14.0	16.6	14.3	14.1	14.8
$(n_{\pi1})_{O_9}$	$\sigma^*_{N_8-O_{10}}$	19.7	18.9	20.8	19.4	19.4	18.8
$(n_{\pi1})_{O_{10}}$	$\sigma^*_{C_2-N_8}$	13.8	13.8	15.8	12.8	12.9	14.5
$(n_{\pi1})_{O_{10}}$	$\sigma^*_{N_8-O_9}$	19.7	18.8	20.2	18.1	18.4	18.6
$(n_{\pi2})_{O_{10}}$	$\pi^*_{N_8-O_9}$	176.1	172.2	177.6	148.6	151.1	173.5
$(n_\sigma)_{F_{11}}$	$(Ry*)_{C_3}$		8.6				8.5
$(n_{\pi1})_{F_{11}}$	$\sigma^*_{C_2-C_3}$		7.3				7.3
$(n_{\pi1})_{F_{11}}$	$\sigma^*_{C_3-C_4}$		6.2				7.4
$(n_{\pi2})_{F_{11}}$	$\pi^*_{C_2-C_3}$		21.9				22.0
σ^*_{C2-N8}	$\sigma^*_{C_3-F_{11}}$		16.0				11.0
$(n_\sigma)_{F_{12}}$	$(Ry*)_{C_4}$			9.7			8.6
$(n_{\pi1})_{F_{12}}$	$\sigma^*_{C_3-C_4}$			7.5			7.6
$(n_{\pi1})_{F_{12}}$	$\sigma^*_{C_4-C_5}$			7.3			7.7
$(n_{\pi2})_{F_{12}}$	$\pi^*_{C_4-C_5}$			22.1			20.6
$(n_\sigma)_{F_{13}}$	$(Ry*)_{C_5}$				8.9		8.7
$(n_{\pi1})_{F_{13}}$	$\sigma^*_{C_4-C_5}$				6.2		7.3
$(n_{\pi1})_{F_{13}}$	$\sigma^*_{C_5-C_6}$				6.6		7.5
$(n_{\pi2})_{F_{13}}$	$\pi^*_{C_4-C_5}$				20.2		20.8
$(n_\sigma)_{F_{14}}$	$(Ry*)_{C_6}$					8.8	9.0
$(n_{\pi1})_{F_{14}}$	$\pi^*_{N_1-C_6}$					11.6	11.7
$(n_{\pi1})_{F_{14}}$	$\sigma^*_{C_5-C_6}$					6.0	7.3
$(n_{\pi2})_{F_{14}}$	$\pi^*_{N_1-C_6}$					27.1	27.0
$\pi^*_{N_1-C_6}$	$\pi^*_{C_2-C_3}$	36.7	47.8	54.8	34.3	28.9	40.0
$\pi^*_{N_1-C_6}$	$\pi^*_{C_4-C_5}$	67.9	73.0	90.6	75.9	61.2	90.3

Energies in kcal mol^{-1}

mol^{-1} for the mono fluorinated 2-NPO derivatives in 3, 4, and 5 positions. The three analogous $(n_{\pi2})_F \rightarrow \pi^*_{C=C}$ interactions in 2-NPO-F4 are stabilized by 22.0, 20.6 and 20.8

kcal mol^{-1}. One likely reason for the large stabilization energy of the $(n_{\pi2})_F \rightarrow \pi^*_{C-N}$ charge delocalization of 27.1 kcal mol^{-1} in 2-NPO-6-F and 27.0 kcal mol^{-1} in 2-NPO-F4 is the accentuated acceptor capability of the C–N bond due to the higher electronegativity of the nitrogen atom of 3.1 [56] in comparison to electronegativity of the carbon atom of 2.6. From Table 8, it can additionally be seen that the $E(2)$ values for the lone electron pair transfer from the $(n_{\pi1})_{O_9}$ and $(n_{\pi1})_{O_{10}}$ donor orbitals to the $\sigma^*_{C_2-N_8}$ antibond acceptor orbital, $(n_{\pi1})_{O9,O10} \rightarrow \pi^*_{C_2-N_8}$, vary approximately between 13 and 17 kcal mol^{-1} which indicates the strengthening of the C_2-N_8 bond by such kind of orbital interactions.

NBO deletion analysis

Basically the different deletion options in the NBO analysis allow for the selective zeroing of off-diagonal elements of the Fock-matrix and thus for the elimination of certain hyperconjugative bond/antibond interactions in a considered molecule. First, we employed the NOSTAR algorithm to switch-off all antibonding and Rydberg off-diagonal Fock-matrix elements. This kind of orbital deletion enables the separation of the hyperconjugation stabilizing (Lewis/non-Lewis) interactions and the steric interactions comprising the van der Waals interactions and Pauli exchange repulsion. By applying the B3LYP/6-311++G(df,pd) computational method and utilizing this type of deletion, the structural optimization of all fluorinated 2-NPOs provided the partitioned energy contributions which are shown in Table 9. From this table, it is evident that the most stable monofluoro 2-NPO is the 2-NPO-5-F derivative, where the fluorine substituent is in *para* position to the NO₂ group. A

Table 9 Deletion NBO analysis of 2-NPO-x-F (x = 3, 4, 5, 6, and 3–4–5–6) using the NOSTAR (deletion of all antibond orbitals) and removal of all fluorine bond–antibond interactions

	E_{tot} (Hartree)	E_L (Hartree)	E_{NL} kcal mol^{-1}
2-NPO-3-F	−627.363394350	−625.294127384	−1298.484
2-NPO-4-F	−627.367223024	−625.092460521	−1427.435
2-NPO-5-F	−627.367705211	−625.310480598	−1290.928
2-NPO-6-F	−627.363597303	−625.262728983	−1318.314
2-NPO-F4	−925.135271306	−922.405162214	−1713.169
Deletion of all fluorine interactions			
2-NPO-3-F	−627.363394350	−627.123638325	−150.449
2-NPO-4-F	−627.367223024	−627.196718582	−106.993
2-NPO-5-F	−627.367705211	−627.133228642	−147.136
2-NPO-6-F	−627.363597303	−627.140782753	−139.818
2-NPO-F4	−925.135271306	−924.310897379	−517.302

E_{tot} total interaction energy, E_L energy of idealized Lewis structure (doubly occupied orbitals), $E_{NL} = E_{tot} - E_L$ the non-Lewis or delocalization (deletion) energy (B3LYP/6-311++G(df,pd) was used)

comparison of the Lewis energy for the ideally localized structure, E_L, and the electronic delocalization energy, E_{NL}, for 2-NPO-5-F with those of the remaining monofluorinated 2-NPOs [E_L (or E_{NL}) (2-NPO-5-F) − E_L (or E_{NL}) (2-NPO-x-F)] has revealed that the energy difference, $\Delta(E_L)$, for 2-NPO-3-F, 2-NPO-4-F, and 2-NPO-6-F amounts to −10.3, −136.8, −30.0 kcal mol^{-1} and $\Delta(E_{NL})$ is 7.6, 136.5, 27.4 kcal mol^{-1}, respectively. From these $\Delta(E_L)$ and $\Delta(E_{NL})$ values, it can be concluded that the Lewis energy E_L favors 2-NPO-5-F over all other monofluorinated 2-NPOs which implies that electrostatic and exchange repulsion interactions are predominant in this molecule. Consideration of the $\Delta(E_{NL})$ discloses that 2-NPO-4-F is mainly stabilized by the delocalization of occupied NBOs into vacant antibonding orbitals. Interestingly, parallel trends have been observed for the chlorinated 2-NPOs.

To get deeper insight into the role of the fluorine substituent by the donor–acceptor stabilization of the above discussed fluorinated 2-NPOs, we utilized the element deletion option by zeroing all off-diagonal elements in the Fock-matrix which are related to all fluorine interactions (Table 9). As it can be seen from Table 9, the deletion of all fluorine hyperconjugative interactions in 2-NPO-3-F leads to the highest electronic delocalization energy, E_{del}, of 150.5 kcal mol^{-1}. The smallest E_{del} value of 107 kcal. mol^{-1} (which represents 7.5 % of the total deletion energy that was obtained by using the NOSTAR deletion option) emerges by switching off all fluorine donor–acceptor interactions in 2-NPO-4-F. This peculiar small contribution of the fluorine hyperconjugative interaction to the total delocalization energy manifests that 2-NPO-4-F is mostly stabilized by the donor–acceptor interactions of the remaining NBOs in addition to π-delocalization (conjugation) and dispersion interactions. From Table 9, it can be concluded that generally the fluorine Lewis–non-Lewis interactions play only a moderate role by the stabilization of the listed 2-NPOs except in the case of 2-NPO-F4. In this case, the contribution of the fluorines hyperconjugative stabilizing interactions to the total non-Lewis energy E_{NL} (=E_{del}) amounts to approximately 30 % of the total deletions energy on zeroing all donor–acceptor natural orbital interactions.

AIM analysis

We also analyzed the topological properties of the charge density distribution in all above cited 2-NPOs by applying the quantum theory of atoms in molecules (AIM) which was developed by Bader and others [57–64]. From Bader's AIM theory, valuable information about bonding properties in molecules and the reasons for their structural stability can be concluded. In addition, changes in charge density distribution, $\rho(r)$, mirror the effects of substituents and thus the variation of the Laplacian of the charge density, $\nabla^2\rho(r_c)$ (which is the algebraic sum of the three eigenvalues, λ_1, λ_2, λ_3 of the charge density at a bond point), allows for a three dimensional representation of these effects. Table 10 summarizes some topological properties of $\rho(r)$ (atomic units are used), which we obtained from the AIM analysis for pyridine, pyridine-N-oxide, and 2-NPO. Table 11 shows these properties at all $(3,-1)$[1] bond critical points in the fluorinated derivatives of 2-NPO by applying the B3LYP/6-311++G(df,pd) (for the results obtained from MP2/aug-cc-pVDZ level see Tables S12 and S13).

It is worth to point out that the charge densities at the BCP of the N_1–C_2 and N_1–C_6 are comparable (and vary only slightly) in all fluorinated 2-NPOs which are shown in Table 11. The negative values of the Laplacian, $\nabla^2\rho(r)$ (indicative for the occurrence of shared interaction or covalent bond) of the N_1–C_6, in the 2-NPO-x-F ($x = 3, 4, 5$) derivatives are significantly smaller (by 20–30 %) in comparison to the Laplacian of the N_1–C_2 bond indicating a reduction of the covalency of the N_1–C_6 versus N_1–C_2 bond.

One more peculiarity emerges by the comparison of the ellipticity values, ε_c[2] of the N_1–C_2 and N_1–C_6 bonds within the fluorinated 2-NPOs series in Table 11. This table shows that the ε_c values for the N_1–C_2 bond are evidently larger than those of the N_1–C_6 bond in 2-NPO-x-F ($x = 3, 4, 5$) indicating that the former bond possesses larger π-character than the latter. However, this trend is reversed in 2-NPO-6-F and 2-NPO-F4 demonstrating that the charge concentration in the plane perpendicular to the bond path has become higher in N_1–C_6 than in N_1–C_2.

Further interesting features of the topological analysis of the fluorinated 2-NPOs are related to the N_1–O_7 bond. Strikingly, at the BCP of this bond: (1) the charge density concentration is substantially high, (2) the negative value of the $\nabla^2\rho(r_c)$ is relatively large, (3) the charge density distribution is almost invariant, which elucidates the aforementioned similarity of the N_1–O_7 bond length in all fluoro 2-NPOs (Table 3), and (4) the values of the bond ellipticity are noticeably low. In conclusion, all these features confirm that the N_1–O_7 bond is predominantly covalent and is of cylindrical symmetry (single bond).

---

[1] The first number indicates the number of non-zero eigenvalues (curvatures) of the Hessian matrix of $\rho_{bcp}(r)$ (the rank of this matrix) and the second number represents the signature of the matrix which is the algebraic sum of the signs of the eigenvalues.

[2] The ellipticity, ε_c, is defined as $\varepsilon_c = \lambda_1/\lambda_2 - 1$ and is considered as a measure for the deviation of the charge distribution in a bond from the cylindrical symmetry (where $\lambda_1 = \lambda_2$ and $\varepsilon_c = 0$) and, therefore, it is used as a measure for the amount of π-character of a bond, and thus the charge concentration perpendicular to the bond path. In ethylene where $|\lambda_2| < |\lambda_1|$ and ε_c is approximately 0.45 depending on the applied computational method and basis set.

Table 10 Atomic and critical point properties of some bonds of pyridine, pyridine-*N*-oxide, 2-nitropyridine-*N*-oxide (2-NPO) as obtained from the B3LYP/6-311++G(df,pd) method

	r_A	r_B	$\rho(r_c)$	λ_1	λ_2	λ_3	$\nabla^2\rho(r_c)$	ε_c
Pyridine								
$N_1–C_2$	1.606	0.917	0.348	−0.761	−0.686	0.456	−0.991	0.11
$C_2–C_3$	1.320	1.310	0.320	−0.695	−0.575	0.304	−0.966	0.21
$C_3–C_4$	1.303	1.323	0.319	−0.683	−0.576	0.296	−0.963	0.19
Pyridine-N-oxide								
$N_1–C_2$	1.690	0.897	0.315	−0.661	−0.556	0.542	−0.675	0.19
$C_2–C_3$	1.338	1.268	0.325	−0.706	−0.571	0.284	−0.993	0.24
$C_3–C_4$	1.331	1.298	0.317	−0.678	−0.569	0.296	−0.951	0.19
$N_1–O_7$	1.179	1.232	0.442	−1.097	−1.020	1.371	−0.746	0.08
2−NPO								
$N_1–C_2$	1.660	0.933	0.320	−0.726	−0.530	0.413	−0.844	0.37
$C_2–C_3$	1.389	1.218	0.323	−0.693	−0.559	0.271	−0.980	0.24
$C_3–C_4$	1.340	1.277	0.321	−0.686	−0.573	0.289	−0.970	0.20
$C_4–C_5$	1.302	1.333	0.316	−0.672	−0.570	0.298	−0.944	0.18
$C_5–C_6$	1.260	1.338	0.328	−0.713	−0.576	0.280	−1.010	0.24
$N_1–C_6$	1.700	0.899	0.309	−0.637	−0.541	0.538	−0.641	0.18
$N_1–O_7$	1.169	1.221	0.454	−1.120	−1.044	1.386	−0.778	0.07
$C_2–N_8$	1.106	1.674	0.272	−0.587	−0.521	0.334	−0.774	0.13
$N_8–O_9$	1.083	1.212	0.521	−1.391	−1.231	1.411	−1.211	0.13
$N_8–O_{10}$	1.094	1.218	0.510	−1.360	−1.203	1.417	−1.143	0.13

All quantities are in atomic units. r_A and r_B are the distances from the nuclei A and B, respectively, to the A–B bond critical point. For $\rho(r_c)$, λ_1, λ_2, λ_3, $\nabla^2\rho(r_c)$, and ε_c see text

As it was alluded to earlier in this work, the reactivity of the C–NO$_2$ bond within nitro aromatics has been the focal point of a vast number of publications which were devoted to the investigation of the role, which the C–NO$_2$ bond plays in energetic materials and highly reactive chemical systems [46, 47]. The NBO analysis has shown that the C–NO$_2$ bond is mainly stabilized by the $(n_{\pi 1})_{O_{9,10}} \rightarrow \sigma^*_{C_2–N_8}$ orbital interactions. Now, a consideration of the AIM results in Table 11 reveals that remarkably the charge density distribution at BCP of the C$_2$–N$_8$ bond remains unaffected by the fluorination in all fluoro 2-NPOs. The small value of the charge density of 0.27e/a_0^3 (1.82 eÅ^{-3}) and the relatively low value of the Laplacian distribution of −0.76 to −0.78 e/a_0^5 (−18.3 to −18.8 eÅ^{-5}) at the BCP of the C–NO$_2$ bond in all fluorinated 2-NPOs indicate that the charges in the C–NO$_2$ bonds are appreciably depleted which is a clear evidence for the accentuated weakness of this bond in comparison to all other bonds in the fluoro 2-NPO series. In addition, the anisotropic charge distribution in these N=O bonds mirrored by the deviation of the ellipticity values from the typical value for a cylindrical charge distribution demonstrates the π character of this bond. From the aforementioned, it becomes apparent that all 2-NPOs (fluorinated and non-fluorinated) exhibit

C–NO$_2$ bonding properties, which classify them to be potential energetic materials. They possess a weak C–NO$_2$ bond that is ready to rupture upon exposure to an external shock which confers such kind of material higher impact sensitivity. Besides, it should be noted that more accurate assessment of the impact sensitivity of the 2-NPOs presented in this work could be achieved by investigating the electrostatic potentials formed by the nuclei and electrons on the surface of a molecule. Such correlation between the impact sensitivity and the electrostatic potential has been excessively studied by Politzer et al. [65, 66].

From Table 11, it also emerges that the positive values of the Laplacian $\nabla^2\rho(r)$ (the positive eigenvalue λ_3 is prevalent) in addition to the relatively low concentration of the charge density $\rho(r_c)$ at the BCPs of the C–F bonds in 2-NPO-3-F, 2-NPO-4-F, and 2-NPO-5-F characterize the local depletion of charges (closed-shell interaction) and thus indicates the polarity of this bond. It is somehow surprising that the values of the charge densities remain almost constant at the BCPs which denotes that the C–F bond strength in these fluorinated 2-NPOs is apparently independent of its position on the heteroaromatic ring. This finding is reflected by the similar values of the C–F bond length in these 2-NPOs (Table 3). The slightly increase of

Table 11 Atomic and critical point properties of some bonds of 2-nitropyridine-N-oxide-x-fluoro (x = 3, 4, 5, 6, and 3–4–5–6–tetra-fluoro) as obtained from the B3LYP/6-311++G(df,pd) method

	r_A	r_B	$\rho(r_c)$	$\nabla^2\rho(r_c)$	ε_c
2-NPO-3-F					
N_1–C_2	1.653	0.929	0.324	−0.842	0.41
C_2–C_3	1.322	1.288	0.327	−0.995	0.36
C_3–C_4	1.402	1.208	0.326	−1.010	0.25
C_4–C_5	1.312	1.321	0.314	−0.931	0.19
C_5–C_6	1.269	1.331	0.327	−0.999	0.24
N_1–C_6	1.702	0.892	0.309	−0.596	0.19
N_1–O_7	1.172	1.221	0.452	−0.767	0.07
C_2–N_8	1.128	1.660	0.271	−0.764	0.04
N_8–O_9	1.082	1.213	0.521	−1.212	0.13
N_8–O_{10}	1.084	1.214	0.520	−1.201	0.13
C_3–F	0.830	1.688	0.273	0.195	0.05
2-NPO-4-F					
N_1–C_2	1.653	0.937	0.322	−0.865	0.37
C_2–C_3	1.377	1.230	0.322	−0.966	0.25
C_3–C_4	1.266	1.341	0.328	−1.015	0.26
C_4–C_5	1.362	1.262	0.323	−0.992	0.24
C_5–C_6	1.270	1.326	0.327	−0.996	0.25
N_1–C_6	1.695	0.904	0.311	−0.678	0.18
N_1–O_7	1.176	1.221	0.449	−0.748	0.07
C_2–N_8	1.116	1.666	0.272	−0.776	0.12
N_8–O_9	1.082	1.211	0.523	−1.217	0.13
N_8–O_{10}	1.093	1.217	0.511	−1.148	0.13
C_4–F	0.832	1.695	0.269	0.215	0.04
2-NPO-5-F					
N_1–C_2	1.667	0.934	0.316	−0.817	0.39
C_2–C_3	1.377	1.230	0.323	−0.977	0.24
C_3–C_4	1.330	1.285	0.320	−0.959	0.20
C_4–C_5	1.230	1.394	0.323	−0.996	0.23
C_5–C_6	1.333	1.265	0.332	−1.035	0.32
N_1–C_6	1.695	0.900	0.311	−0.643	0.23
N_1–O_7	1.164	1.218	0.459	−0.802	0.08
C_2–N_8	1.106	1.669	0.273	−0.775	0.15
N_8–O_9	1.083	1.211	0.522	−1.209	0.13
N_8–O_{10}	1.097	1.217	0.509	−1.129	0.13
C_5–F	0.831	1.693	0.270	0.199	0.08
2-NPO-6-F					
N_1–C_2	1.665	0.929	0.318	−0.815	0.36
C_2–C_3	1.396	1.206	0.323	−0.983	0.25
C_3–C_4	1.332	1.288	0.320	−0.962	0.20
C_4–C_5	1.291	1.339	0.316	−0.942	0.19
C_5–C_6	1.181	1.413	0.329	−1.023	0.28
N_1–C_6	1.651	0.953	0.321	−0.941	0.38
N_1–O_7	1.173	1.216	0.452	−0.746	0.06
C_2–N_8	1.115	1.668	0.272	−0.775	0.11
N_8–O_9	1.082	1.212	0.522	−1.215	0.13
N_8–O_{10}	1.093	1.217	0.512	−1.153	0.13

Table 11 continued

	r_A	r_B	$\rho(r_c)$	$\nabla^2\rho(r_c)$	ε_c
C_6–F	0.818	1.664	0.288	0.252	0.08
2-NPO-F4					
N_1–C_2	1.659	0.926	0.320	−0.804	0.41
C_2–C_3	1.310	1.295	0.326	−0.982	0.38
C_3–C_4	1.323	1.302	0.326	−0.998	0.36
C_4–C_5	1.303	1.327	0.324	−0.987	0.36
C_5–C_6	1.283	1.329	0.328	−1.002	0.41
N_1–C_6	1.646	0.947	0.324	−0.927	0.45
N_1–O_7	1.179	1.214	0.449	−0.716	0.06
C_2–N_8	1.147	1.645	0.271	−0.756	0.05
N_8–O_9	1.081	1.211	0.523	−1.217	0.13
N_8–O_{10}	1.084	1.212	0.521	−1.202	0.13
C_3–F	0.826	1.676	0.280	0.209	0.01
C_4–F	0.824	1.676	0.279	0.252	0.04
C_5–F	0.825	1.675	0.280	0.225	0.01
C_6–F	0.814	1.654	0.294	0.277	0.13

All quantities are in atomic units. r_A and r_B are the distances from the nuclei A and B, respectively, to the A–B bond critical point. For $\rho(r_c)$, $\nabla^2\rho(r_c)$, and ε_c see text

the charge accumulation at the BCP of the C_6–F bond in 2-NPO-6-F and 2-NPO-F4 in comparison to the C–F bond in the remaining fluoro 2-NPOs (Table 11) and the mixing of π character as a result of fluorine lone pair donation in this bonding orbitals justify the strengthening of this bond. As it was shown above in this work (Table 3) the C_6–F bond length in these two fluorinated 2-NPOs is significantly shorter than the C–F bonds in the remaining fluoro 2-NPOs which confirms this way of elucidation.

Aromaticity of 2-NPO and its fluorinated derivatives

To investigate the extent to which the aromaticity of the pyridine-N-oxide is affected by the strong charge withdrawing substituents NO_2 and F and their relative positions to the N-oxide fragment we calculated the nuclear independent chemical shift NICS(1) which is defined as the averaged negative isotropic shielding (in ppm) at 1 Å above the ring plane [67–69]. All NICS values were computed by employing the standard GIAO method implemented in the Gaussian09 software package by using the HF and B3LYP wave functions in combination with the 6-311++G(df,pd), and aug-cc-pVDZ basis sets.

In order to approximately separate the contributions of the nitro group and the fluorine substitution to the alteration of the aromaticity of the pyridine-N-oxide system, we also calculated the NICS (1) values for various x-F-pyridine-N-oxides (x = 2, 3, 4) in addition to 3,4,5,6-tetrafluoro-pyridine-N-oxide and penta-fluoro-pyridine-N-oxide.

Table 12 Calculated NICS (ppm) values for 2-nitropyridine-*N*-oxide (2-NPO) and pyridine-*N*-oxide (PO) and some of their fluorinated derivatives (see text). HF/6-311++G(df,pd) was used

Compounds	NICS(1)	NICS(1)$_{zz}$
Pyridine	−11.3	−31.9
Pyridine-*N*-oxide	−11.7	−30.4
2-NPO	−11.6	−22.7
2-NPO-3-F	−12.1	−22.9
2-NPO-4-F	−10.9	−22.7
2-NPO-5-F	−12.5	−27.9
2-NPO-6-F	−11.9	−27.0
2-NPO-F4	−12.7	−27.4
2-F-PO	−12.5	−30.0
3-F-PO	−11.5	−28.5
4-F-PO	−10.6	−27.0
5-F-PO	−11.5	−28.5
6-F-PO	−12.5	−30.0
F4-PO	−11.8	−25.2
F5-PO	−12.0	−24.6

From the NICS(1) values in Table 12, it can be generally concluded that neither the N-oxidation of pyridine nor its nitration or fluorination noticeably affects the aromaticity of the parent molecule. These values also reveal that the 2-NPO-F4 exposes the largest aromatic character followed by 2-NPO-5-F, 2-NPO-3-F, 2-NPO-6-F, and 2-NPO-4-F, respectively. As Table 12 additionally shows the non-fluorinated compounds, pyridine-*N*-oxide and 2-NPO, exhibit almost the same degree of aromaticity as in pyridine indicating the little influence of the diatropicity of pyridine ring by N-oxidation and nitration in *ortho* position. A comparison of the NICS(1) values for the fluorinated 2-NPO and pyridine-*N*-oxides (POs) shows that the nitro group leads to a slight increase of the electron delocalization and thus to higher aromatic character (diatropicity) of the fluorinated pyridine-*N*-oxides. One exception within this series of compounds is provided by the fluorination in *ortho* position where the NICS(1) value slightly decreases (by 0.6 ppm) upon nitration. However, it should be noted that all differences of the NICS(1) value which are less than 1 ppm are marginal and lie within the uncertainty limits of these values. Aside from that, the NICS index has generally proven to be to some extent dependent on the computational level of theory. For example although the trend of the NICS(1) values which have been obtained from the B3LYP/6-311++G(df,pd) (Table S14) is roughly consistent with the HF/6-311++G(df,pd) results, however, the density functional method predicts a decrease of the aromaticity of the pyridine ring upon N-oxidation (NICS(1) for pyridine is −10.4 and for pyridine-*N*-oxide −8.8) and a slight increase of the aromaticity of pyridine-*N*-oxide on

nitration in *ortho* position to the N-oxide group (Table S14).

Without going into further details, it is of importance to note that in a vast number of papers it has been elaborately shown that (depending on the size of the ring) the in-plane aromaticity which is indicated by the isotropic NICS(0) value contains considerable contribution of in-plane σ-aromaticity resulting from the diamagnetic shielding of the σ electronic framework. Although the NICS(1) value is a better descriptor of the π contribution to aromaticity due to the apparent decrease of the local contributions of the σ framework at larger distances from the ring center, however, this value is still related to the total isotropic shielding and thus is contaminated by σ contributions. A largely separation of the σ aromaticity from the out-of-plane π aromaticity was achieved by the introduction of new NICS descriptor which considers the out-of-plane zz components of the shielding tensor elements at a certain distance *n* in Å above the ring plane designated as NICS(*n*)$_{zz}$. NICS(1)$_{zz}$ is defined as the MO contribution to the zz component of the shielding tensor perpendicular to the ring plane. Since this NICS$_{zz}$ index still incorporates some non-π contributions a new more specific measure for the pure π-aromaticty was introduced (NICS$_{\pi zz}$) which takes into account only the π contributions to the out-of-plane NICS tensor component arising from the canonical molecular orbitals with π character [69, 70]. However, on various occasions it has been pointed out that NICS(1)$_{zz}$ is easily computable and is an excellently performing aromaticity descriptor. Therefore, it represents an adequate substitute for NICS$_{\pi zz}$ [70]. Moreover, recently it was also shown that the NICS(1)$_{zz}$ value denotes the highest degree of aromaticity for aromatic systems [71]. Based on these observations we focused on the NICS(1)$_{zz}$ index to elucidate the variation of the degree of aromaticity in all fluorinated and non-fluorinated 2-NPOs and pyridine-*N*-oxides. Assuming that the non-planarity of some of the compounds which are displayed in Table 12 has only marginal effect on the NICS$_{zz}$ tensor component perpendicular to the ring plane, the following conclusions can be derived from the evaluation of the NICS(1)$_{zz}$ values for these compounds: (a) An apparent reduction of the degree of π aromaticity upon N-oxidation and nitration of pyridine is indicated by the less negative values of NICS$_{zz}$. (b) The fluorination of 2-NPO in 3 and 4 positions has no influence on the aromaticity of this molecule. (c) The fluorination in *para* position to the nitro group exhibits the highest degree of aromaticity within the fluorinated 2-NPOs indicating the largest π electron delocalization and the *para* directionality of the fluorine substituent. (d) There is almost no difference between the aromaticity of 2-NPO-6-F and 2-NPO-F4 which may be interpreted in terms of charge

delocalization in these two molecules that is predominantly caused by the fluorine substituent in *ortho* position to the N-oxide moiety.

It is worth to point out that a noticeable discrepancy exists between the trends of the alteration of the aromaticity on moving from one homologue to the other mirrored by the NICS(1) and NICS(1)$_{zz}$ values (Tables 12 and S14). However, the variation of the latter NICS index reflects more reliably the influence of the substitution on the aromaticity of these heterocyclic systems since it is dominated by π contributions to the NICS$_{zz}$ tensor.

Finally, a comparison between the NICS(1)$_{zz}$ values for the monofluorinated pyridine-*N*-oxides and 2-NPOs unveils that the aromaticity decreases as a result of nitration signifying the electron withdrawing ability of the nitro group and the partial localization of the π electrons.

Summary and conclusions

This study has generally shown that in all fluorinated and non-fluorinated nitropyridine-N-oxides the choice of the model chemistry has considerable effect on both the structures and potential functions of the internal rotation of the NO$_2$ group. For instance using MP2/cc-pVDZ provided an +*sc*/−*ac* arrangement of the NO$_2$ group in 2-NPO and a non-planar ring with a puckering amplitude of $Q = 0.018$ Å. However, the augmentation of the basis set with diffuse functions led to a *clinal* arrangement where the NO$_2$ plane is perpendicular to the ring plane and to a planar ring.

To explore the impact of the direct adjacency of the nitro group and the N-oxide moiety and to gain more insight into the nature of the mutual interaction between these electron-rich groups, we studied the structures of 3-NPO and 4-NPO where the nitro group is further apart from the N-oxide fragment. The structure of PNPO was also optimized to inspect the effect of the nitro groups crowding. The proximity of five electron-rich substituents like the nitro group has forced the ring to pucker resulting in a puckering amplitude of $Q = 0.028$ Å.

Mainly intramolecular interactions of various kinds and charge redistribution as a result of substitution have been made accountable for the chemical reactivity, remarkable magnetic and optical properties as well as the versatile biological activity. We, however, pointed out that the enforced disruption of the planarity of these heterocyclic compounds and the resulting extra strain play a prominent role by the enhancement of the chemical and biological activity of this class of molecules, e.g. impact sensitivity for characterizing high energy density materials and genotoxicity.

Following additional conclusions can be drawn from this work:

1. Remarkably, the successive fluorination of 2-NPO has little influence on its geometrical parameters. On the other hand, while the C–F bond in 2-NPO-3-F, 2-NPO-4-F, and 2-NPO-5-F remains essentially unaffected this bond shortens significantly by 0.019 Å in 2-NPO-6-F. This bond contraction is due to hyperconjugative interactions with the neighboring N-oxide fragment which has been confirmed by the NBO analysis and the delocalization energy calculated by SOPT.

2. A large variety of NPOs with different kinds of substituents like F, Cl, CH$_3$ and additional NO$_2$ groups has been examined in order to get more insight into the reasons leading to the alteration of the structure, aromaticity and the intramolecular stabilizing or destabilizing interactions between substituent/heteroaromatic ring and between substituents themselves including the N-oxide fragment.

3. Analogous to the known relationship between the total Mulliken charges of the NO$_2$ group, Q_{NO_2}, and the conformational stability and structures of a variety of nitrobenzene derivatives, we introduced the corresponding total charges for the pyridine ring, (Q_{ring}), and methyl group (Q_{CH_3}). For forming these total charges, we used the less basis set-dependent natural charges. It was shown that the group charges, Q, are basically indicative for occurring electronic effects, but they do not provide indications of directionality of substitution on the heteroaromatic ring since due to their inductive or resonance effects and their relative positions to each other. All these factors may lead to additive or opposing subtracting effects which dictate the reactivity of ring in the NPOs molecular systems and its readiness for electrophilic or nucleophilic attack.

4. This work has also shown that the variation of the basis set and its augmentation with diffuse functions (and in some instances the alteration of the wave function as well) has tremendous impact on the profile, conformational stability and the barrier height for internal rotation of the NO$_2$ group. The computational results clearly demonstrate that particular caution should be exercised when investigating energy minima on the potential energy hypersurface by performing quantum mechanical calculations and applying various basis sets (and wave functions) at different levels of theory.

5. Not only the size of the selected basis set has profound influence on the potential barrier for internal rotation of the nitro group but also the fluorine substitution. Hyperconjugative interactions as well as electrostatic and Pauli-exchange repulsive interactions (steric effects) are accountable for the alteration of the potential barrier within the fluorinated heteroaromatics which have been presented in this study.

6. Switching off all antibonding and Rydberg off-diagonal Fock-matrix elements (NOSTAR deletion) in the NBO space has revealed that 2-NPO-5-F is the most stable molecule among the monofluorinated 2-NPOs. From the $\Delta(E_L)$ values for the variety of fluorinated 2-NPOs, it was concluded that the Lewis energy E_L favors 2-NPO-5-F over the other homologues. Consideration of $\Delta(E_{NL})$ values revealed that 2-NPO-4-F is mainly stabilized by the delocalization of occupied NBOs into vacant antibonding orbitals. Interestingly, parallel trends have been observed for the chlorinated 2-NPOs.

7. One of the focal points of this study was the scrutiny of the C–NO$_2$ bond in the fluorinated and non-fluorinated 2-NPOs. As generally accepted, this bond plays a key role by the determination of the impact sensitivity of energetic [26–28] and genotoxic [6] materials. The NBO analysis has shown that the C–NO$_2$ bond is mainly stabilized by the $(n_{\pi 1})_{O_{9,10}} \rightarrow \sigma^*_{C_2-N_8}$ orbital interactions. From the AIM results in Table 11, it was apparent that the charges in the C–NO$_2$ bond in all fluorinated 2-NPOs are appreciably depleted which is a clear evidence for the accentuated weakness of this bond. From these results, it became apparent that all 2-NPOs (fluorinated and non-fluorinated) exhibit particular C–NO$_2$ bonding properties which classify them to be potential energetic materials (with high impact sensitivity).and perhaps biologically active agents.

8. Our calculations showed that the C–NO$_2$ bond length is fairly dependent on the employed level of theory; therefore, it is not appropriate to consider the computed C–NO$_2$ bond length for the assessment of the impact sensitivity of energetic materials. Also the known correlation between the C-NO$_2$ bond length and the barrier height for internal rotation of the nitro group (the shorter this bond the higher is the potential barrier) should be considered with caution (at least in similar heteroaromatics presented in this work).

9. Finally, two essential remarks have to be made concerning the topological properties of the charge density distribution and the various conclusions which have been derived from them: (1) The classification of bonds in shared interactions (covalent bond) and closed-shell interactions (polar or ionic bonds) and the consideration of the bond ellipticity as a measure for the extent of the π character contribution to a bond are not strictly direct consequences of the AIM quantum theory but only based on trends observed in the results which were obtained from a large number of theoretical calculations [64]. (2) These properties are inconsistent upon the variation of the level of the computational method in use.

References

1. Malkov AV, Bell M, Castelluzzo F, Kocovsky P (2005) Org Lett 7:3219
2. Balzarini J, Stevens M, de Clercq E, Schols D, Pannecouque C (2005) J Antimicrobial Chemother 55:135
3. Balzarini J, Stevensand M, Andrei G (2002) Helv Chim Acta 85:2961–2974
4. Balzarini J, Keyaerts E, Vijgen L, Fandermeer F, Stevens M, de Clercq E, Egberink H, van Ranst M (2006) J Antimicrobial Chemother 57:472
5. Ochiai E (1977) Aromatic amine oxides. Elsevier, Amsterdam
6. Teasdale A (ed) (2011) Genotoxic impurities, strategies for identification and control. Wiley, Hoboken
7. Albini A, Pietra S (1991) Heterocyclic N-oxides. CRC Press, Boca Raton
8. Albini A (1993) Synthesis 263
9. Anderson H, Wang X, Bjorklund M, Olson R, Almqvist F (2007) Tetrahedron Lett 248:6941
10. Kanyiva KS, Naka Y, Hiyama T (2007) Angew Chem Int Ed 46:8872
11. Keith JM (2006) J Org Chem 71:9540
12. Ponomarenko SP, Borovikov YJ, Pivovarova NS, Borovikov GS, Makoveckii VP (1993) Zh Obshch Khim 53:1872
13. Chemla DS, Zyss J (eds) (1987) Nonlinear optical properties of organic molecules and crystals. Academic Press, New York
14. Zyss J (ed) (1994) Molecular nonlinear optics. Academic Press, New York
15. Optical Nonlinearities in Chemistry Chem Rev (1994) 1:94
16. Verbiest T, Houbrechts S, Kauranen M, Claes K, Persoons A (1997) J Mater Chem 7:2175
17. Dalton LR, Harper AW, Ghosn R, Steier WH, Ziari M, Fetterman H, Shi Y, Mustacich RV, Jen AKY, Shea KJ (1995) Chem Mater 7:1060
18. Pøcaut J, Fur YL, Levy JP, Masse R (1993) J Mater Chem 3:333
19. Xu D, Liu MG, Hou WB, Yuan DR, Jiang MH, Ren Q, Chai BHC (1994) Mater Res Bull 29:73
20. Frisch MJ, Trucks GW, Schlegel HB, Scuseria GE, Robb MA, Cheeseman JR, Scalmani G, Barone V, Mennucci B, Petersson GA, Nakatsuji H, Caricato M, Li X, Hratchian HP, Izmaylov AF, Bloino J, Zheng G, Sonnenberg JL, Hada M, Ehara M, Toyota K, Fukuda R, Hasegawa J, Ishida M, Nakajima T, Honda Y, Kitao O, Nakai H, Vreven T, Montgomery Jr. JA, Peralta JE, Ogliaro F, Bearpark M, Heyd JJ, Brothers E, Kudin KN, Staroverov VN, Kobayashi R, Normand J, Raghavachari K, Rendell A, Burant JC, Iyengar SS, Tomasi J, Cossi M, Rega N, Millam JM, Klene M, Knox JE, Cross JB, Bakken V, Adamo C, Jaramillo J, Gomperts R, Stratmann RE, Yazyev O, Austin AJ, Cammi R, Pomelli C, Ochterski JW, Martin RL, Morokuma K, Zakrzewski VG, Voth GA, Salvador P, Dannenberg JJ, Dapprich S, Daniels AD, Farkas Ö, Foresman JB, Ortiz JV, Cioslowski J, Fox DJ (2009) Gaussian 09, revision B.01. Gaussian, Inc., Wallingford, CT
21. Werner HJ, Knowles PJ, Knizia G, Manby FR, Schütz M, Celani P, Korona T, Lindh R, Mitrushenkov A, Rauhut G, Shamasundar KR, Adler TB, Amos RD, Bernhardsson A, Berning A, Cooper DL, Deegan MJO, Dobbyn AJ, Eckert F, Goll E, Hampel C, Hesselmann A, Hetzer G, Hrenar T, Jansen G, Köppl C, Liu Y, Lloyd AW, Mata RA, May AJ, McNicholas SJ, Meyer W, Mura ME, Nicklaß A, O'Neill DP, Palmieri P, Pflüger K, Pitzer R, Reiher M, Shiozaki T, Stoll H, Stone AJ, Tarroni R, Thorsteinsson T, Wang M, Wolf A

MOLPRO is a package of ab initio programs. Molpro Version 2009.1

22. Cremer D, Pople JA (1975) J Am Chem Soc 97:1354
23. Cremer D, Pople JA (1975) J Am Chem Soc 97:1358
24. Cremer D (1990) J Phys Chem 94:5502
25. Haasnoot CAG (1992) J Am Chem Soc 114:882
26. Andres G, Borges I Jr (2011) J Phys Chem 114:9055
27. Murray JS, Lane P, Politzer P (1998) Mol Phys 93:187
28. Murray JS, Lane P, Politzer P (1995) Mol Phys 85:1
29. Li J, Huang Y, Dong H (2005) J Energy Mater 23:133
30. Chiang JF, Song JJ (1982) J Mol Struct 96:151
31. Grimme S, Huenerbein R, Ehrlich S (2011) Chem Phys Chem 12:1258
32. Reed AE, Weinstock RB, Weinhold F (1985) J Chem Phys 83:735
33. Mulliken RS (1955) J Chem Phys 23:1833, 2343
34. Maseras F, Morokuma K (1992) Chem Phys Lett 195:500
35. Guerra CF, Handgraaf JW, Baerends EJ, Bickelhaupt FM (2004) J Comput Chem 25:1899
36. Olson RM, Marenich AV, Cramer CJ, Truhlar DG (2007) J Chem Theory Comput 3:2046
37. Bickelhaupt FM, Hommes N, Guerra C, Baerends E (1996) Organometallics 15:2923–2931
38. Ishikawa S, Madjarova G, Yamabe T (2001) J Phys Chem B 105:11986–11993
39. Gross KC, Seybold PG, Hadad CM (2002) Int J Quantum Chem 90:445–458
40. Zhang C, Shu Y, Huang Y, Zhao X, Dong H (2005) J Phys Chem B 109:8978–8982
41. Zhang C, Shu Y, Huang Y, Zhao X, Wang X, Dong H (2004) Sci Technol Energy Mater 65:191–196
42. Zhang C (2009) J Hazard Mater 161:21–28
43. Zhang C (2008) Propellants Explos Pyrotech 33:139–145
44. Kamlet MJ, Adolph HG (1979) Propellants Explos Pyrotech 4:30–34
45. Yau AD, Byrd EFC, Rice BM (2009) J Phys Chem A 113:6166–6171
46. Chen PC, Chen SC (2001) Int J Quantum Chem 83:332
47. Chen PC, Lo W, Hu KH (1997) Theor Chim Acta 95:99
48. Staikova M, Csizmadia IG (2001) J Mol Struct 476:181
49. van Lenthe JH, de Rijdt JGCM, van Duijneveldt FB (1987) Adv Chem Phys 69:521
50. van Mourik T (2009) In: Law MM, Ernesti A (eds) Molecular potential energy surface in many dimensions. CCP6, Daresbury Laboratory, Warrington, p 10
51. Weinhold F, Landis CR (2005) Valency and bonding: a natural bond orbital donor-acceptor perspective. Cambridge University Press, Cambridge
52. Weinhold F (1998) In: Schleyer PVR, Allinger NL, Clark T, Gasteiger J, Kollman PA, Schaefer HF III, Schreiner PR (eds) Encyclopedia of computational chemistry, vol 3. Wiley, Chichester, pp. 1792–1811
53. Reed AE, Weinhold F (1985) J Chem Phys 83:1736
54. Reed AE, Curtiss LA, Weinhold F (1988) Chem Rev 88:899
55. King BF, Weinhold F (1995) J Chem Phys 103:333
56. Suresh CH, Koga N (2002) J Am Chem Soc 124:1790–1797
57. Bader RFW (1990) Atoms in molecules—a quantum theory. Oxford University Press, Oxford
58. Bader RFW (1998) In: Schleyer PVR (ed) Encyclopedia of computational chemistry, vol 1. Wiley, New York, p 64
59. Bader RFW (1991) Chem Rev 91:893
60. Wiberg KB, Breneman CM (1990) J Am Chem Soc 112:8765
61. Bader RFW (1985) Acc Chem Res 18:9
62. Wiberg KB, Bader RFW, Lau CDH (1987) J Am Chem Soc 109:985
63. Bader RFW, Slee TS, Cremer D, Kraka E (1983) J Am Chem Soc 105:5061
64. Bader RFW, Essén H (1984) J Chem Phys 80:1943
65. Politzer P, Lane P, Murray JS (2011) Cent Eur J Energy Mater 8:39–52
66. Murray JS, Concha MC, Politzer P (2009) Mol Phys 107:89–97
67. PvR Schleyer, Maerker C, Dransfeld A, Jiao H, NJRvE Hommes (1996) J Am Chem Soc 118:6317
68. Corminboeuf C, Heine T (2003) J Am Chem Soc 125:13930
69. Corminboeuf C, Heine T, Seifert G, PvR Schleyer, Weber J (2004) Phys Chem Chem Phys 6:273–276
70. Fallah-Bagher-Shaidaei H, Wannere CS, Corminboeuf C, Puchta R, PvR Schleyer (2006) Org Lett 8:863–866
71. Stanger A (2006) J Org Chem 71:883–893